Fat-containing Retroperitoneal Lesions: Imaging Characteristics, Localization, and Differential Diagnosis[1]

Akram M. Shaaban, MBBCh
Maryam Rezvani, MD
Marc Tubay, MD
Khaled M. Elsayes, MD
Paula J. Woodward, MD
Christine O. Menias, MD

Abbreviations: AML = angiomyolipoma, GCT = germ cell tumor, RCC = renal cell carcinoma

RadioGraphics 2016; 36:710–734

Published online 10.1148/rg.2016150149

Content Codes: CT GU MR US

[1]From the Department of Radiology, University of Utah, 30 North 1900 East, 1A71, Salt Lake City, UT 84132 (A.M.S., M.R., P.J.W.); Imaging Department, U.S. Air Force Academy Medical Clinic, USAF Academy, Colorado Springs, Colo (M.T.); Department of Radiology, University of Texas MD Anderson Cancer Center, Houston, Tex (K.M.E.); and Department of Radiology, Mayo Clinic, Scottsdale, Ariz (C.O.M.). Presented as an education exhibit at the 2014 RSNA Annual Meeting. Received June 17, 2015; revision requested September 30 and received October 17; final version accepted December 2. For this journal-based SA-CME activity, the author M.T. has provided disclosures; all other authors, the editor, and the reviewers have disclosed no relevant relationships. **Address correspondence to** A.M.S. (e-mail: *akram.shaaban@hsc.utah.edu*).

SA-CME LEARNING OBJECTIVES

After completing this journal-based SA-CME activity, participants will be able to:

- Define imaging signs that may help identify the organ of origin for a retroperitoneal mass.
- Identify the appearance of fat at CT, MR imaging, and US.
- Describe the demographic, clinical, and imaging characteristics of specific fat-containing retroperitoneal masses.

See www.rsna.org/education/search/RG.

The complex anatomy of the retroperitoneum is reflected in the spectrum of neoplastic and nonneoplastic conditions that can occur in the retroperitoneum and appear as soft-tissue masses. The presence of fat within a retroperitoneal lesion is helpful in refining the differential diagnosis. Fat is easily recognized because of its characteristic imaging appearance. It typically is hyperechoic at ultrasonography and demonstrates low attenuation at computed tomography (−10 to −100 HU). Magnetic resonance imaging is a more ideal imaging modality because it has better soft-tissue image contrast and higher sensitivity for depicting *(a)* microscopic fat by using chemical shift imaging and *(b)* macroscopic fat by using fat-suppression techniques. Whether a lesion arises from a retroperitoneal organ or from the soft tissues of the retroperitoneal space (primary lesion) is determined by examining the relationship between the lesion and its surrounding structures. Multiple imaging signs help to determine the organ of origin, including the "beak sign," the "embedded organ sign," the "phantom (invisible) organ sign," and the "prominent feeding artery sign." Adrenal adenoma is the most common adrenal mass that contains microscopic fat, while myelolipoma is the most common adrenal mass that contains macroscopic fat. Other adrenal masses, such as pheochromocytoma and adrenocortical carcinoma, rarely contain fat. Renal angiomyolipoma is the most common fat-containing renal mass. Other fat-containing renal lesions, such as lipoma and liposarcoma, are rare. Fatty replacement of the pancreas and pancreatic lipomas are relatively common, whereas pancreatic teratomas are rare. Of the primary retroperitoneal fat-containing lesions, lipoma and liposarcoma are common, while other lesions are relatively rare.

Introduction

The retroperitoneum is a complex space that contains solid organs and hollow viscera, lymphatics and lymph nodes, major vascular structures, and stromal tissues of the retroperitoneum. The complex anatomy of the retroperitoneum is reflected in the numerous neoplastic and nonneoplastic conditions that can occur in this space, which appear as soft-tissue masses. Identification of a retroperitoneal mass at imaging is a challenging task for radiologists, who depend on a combination of clinical, laboratory, and imaging features to compile a list of differential possibilities. The presence of fat within a retroperitoneal lesion is helpful in refining the differential diagnosis (Table 1). Fat is easily recognized because of its characteristic imaging appearance. Although ultrasonography (US) is rarely used for characterization of retroperitoneal masses, a large mass may be detected initially at US. Although the echogenicity of fat can be

TEACHING POINTS

- Chemical shift imaging (with in-phase and out-of-phase sequences) is the most reliable MR imaging technique for diagnosing adrenal adenomas. Most of these lesions demonstrate a decrease in signal intensity on out-of-phase images when compared with in-phase images. A decrease in signal intensity of more than 16.5% is considered diagnostic of an adenoma.
- AMLs with minimal fat are usually hyperattenuating relative to the renal parenchyma on nonenhanced CT images and hypointense on T2-weighted MR images, inherent features that reflect the predominant smooth-muscle component and classically overlap with features of papillary RCC.
- Differentiating renal lipoma or well-differentiated liposarcoma from AML may be difficult: AMLs may contain large aneurysmal vessels, while lipomas and liposarcomas are relatively avascular and rarely occur with multiple lesions, as may be seen with AMLs.
- Retroperitoneal fat necrosis is usually caused by the lipolytic effect of pancreatic enzymes released during acute pancreatitis. It usually is accompanied by pancreatic parenchymal necrosis but can occur without visible pancreatic involvement.
- Splenectomy may have a role in accelerating development of extramedullary hematopoiesis in uncommon sites.

variable at US, it typically is hyperechoic and may demonstrate posterior acoustic shadowing. Computed tomographic (CT) images derive their contrast parameters predominantly from the physical properties of tissue. This, along with the high spatial resolution of CT, provides accurate tissue attenuation measurement. CT attenuation measurements are quantitative, with –10 to –100 HU corresponding to fat. However, CT is limited in the demonstration of mild intracellular fat deposition or small amounts of macroscopic fat. If the fraction of fat within a voxel is small, the mean CT attenuation measurement will not reflect its presence because of volume-averaging effect.

Magnetic resonance (MR) images have lower spatial resolution than CT images but better soft-tissue contrast and greater sensitivity in detection of microscopic fat (1). There are two MR imaging techniques for identification of fat within a structure: fat saturation and chemical shift imaging. Fat saturation is best for diagnosing macroscopic fat, as it requires a greater degree of steatosis. Chemical shift imaging is an ideal technique for identifying microscopic fat or intracellular fat in a lesion or organ. Selective echo delay times are used in T1-weighted gradient-echo imaging sequences to accentuate the chemical shift phenomenon, producing images in which fat and water signals are in phase and opposed phase. Loss of signal intensity on opposed-phase images relative to in-phase images indicates the presence of fat and water within the same voxel and is therefore diagnostic of microscopic fat. The sensitivity and specificity of chemical shift imaging for hepatic steatosis are 81% and 100%, respectively (1).

Determination of the Organ of Origin

It can be difficult to localize large abdominal masses to an anatomic space and to identify the organ of origin. Whether a lesion arises from a retroperitoneal organ or from the soft tissues of the retroperitoneal space (primary retroperitoneal lesion) is based on the relationship between the lesion and its surrounding structures. A mass that is embedded in and completely surrounded by the parenchyma of an organ undoubtedly arises from that organ. However, it is more difficult to determine the origin of a mass at the margin of an organ. The interface of the mass with an adjacent organ can provide insight as to whether it displaces or arises from that organ (Table 2). The "beak sign" relates to the shape of a solid organ at the edge of its interface with an adjacent mass (2). A sharp beak shape implies that the mass arises from the adjacent organ (Fig 1), whereas rounded organ edges suggest displacement by the mass (Fig 2). The "embedded organ sign" refers to the relationship between a mass and a hollow viscus or other adjacent malleable organ (ie, inferior vena cava) (2). If the mass only displaces the organ but does not originate from it, the organ assumes a crescent shape (Fig 3). When the mass encases an organ such that the organ appears to be embedded in it, the mass is presumed to have arisen from the organ (Fig 4). In the latter instance, the organ-tumor interface may be sclerotic with a desmoplastic reaction. The "phantom (invisible) organ sign" is seen when a large mass arises from a small organ such that the organ of origin is obliterated and no longer visible (2). It should be noted, however, that the phantom organ sign might be falsely positive when a small organ is markedly displaced and compressed by a large mass. Lastly, hypervascular retroperitoneal masses may have large feeding arteries that can help identify the organ of origin; this is also known as the "prominent feeding artery sign" (2).

Fat-containing Adrenal Lesions

Adrenal Cortical Adenoma

Adrenal cortical adenoma is the most common adrenal lesion, found in 2%–9% of all autopsies. Most adrenal cortical adenomas measure 2.0–2.5 cm. Rarely, adenomas can appear as larger masses, measuring up to 4 cm (3). They usually are well circumscribed and homogeneous on nonenhanced images and demonstrate homogeneous contrast material enhancement. Adrenal

Table 1: Differential Diagnosis of Fat-containing Retroperitoneal Masses

Organ of Origin	Common Diagnoses	Rare Diagnoses
Adrenal	Adenoma, myelolipoma	Carcinoma, pheochromocytoma, neurogenic tumors, AML, lipoma and liposarcoma, metastasis
Renal	AML	RCC, lipoma and liposarcoma, replacement lipomatosis
Pancreatic	Lipoma, focal pancreatic steatosis	Pancreatic pseudolipohypertrophy, pancreatic teratoma
Primary retroperitoneal	Lipoma and liposarcoma	Myelolipoma, primary and secondary GCTs, neurogenic tumors, lipomatosis, fat necrosis, extramedullary hematopoiesis

Note.—AML = angiomyolipoma, GCT = germ cell tumor, RCC = renal cell carcinoma.

Table 2: Positive Signs Indicating That a Retroperitoneal Tumor Arises from an Adjacent Organ

Sign	Definition
Beak sign	Sharp beak shape of organ of origin occurs at the edge of the interface with the tumor
Embedded organ sign	Organ of origin is encased by the tumor, with or without a sclerotic interface
Phantom (invisible) organ sign	Organ of origin is obliterated by the tumor
Prominent feeding artery sign	Large feeding arteries of a hypervascular tumor point to the organ of origin

adenomas typically contain variable amounts of microscopic fat (intracellular lipid) and can be classified as lipid rich or lipid poor according to the lipid content. The attenuation values of adenomas depend on the amount of lipid. A lipid-rich adenoma is diagnosed when an adrenal lesion measures less than 10 HU on nonenhanced CT images. Lipid-poor adenomas constitute about 10%–40% of adenomas and demonstrate higher attenuation on nonenhanced CT images (4). Threshold values of more than 60% for absolute contrast material washout and 40% for relative contrast material washout have been found to be highly sensitive and specific for diagnosing adrenal adenomas (5). Chemical shift imaging (with in-phase and out-of-phase sequences) is the most reliable MR imaging technique for diagnosing adrenal adenomas. Most of these lesions demonstrate a decrease in signal intensity on out-of-phase images when compared with in-phase images. A decrease in signal intensity of more than 16.5% is considered diagnostic of an adenoma (Fig 5) (6). Rarely, foci of macroscopic fat have been reported in adrenocortical adenomas, resulting in a misdiagnosis of myelolipoma on images. Such lesions were found to be adenomas with myelolipomatous and/or lipomatous changes at postoperative pathologic evaluation (7).

Adrenal Myelolipoma

Myelolipoma is the most common macroscopic fat-containing adrenal mass. Myelolipoma is an uncommon, benign, nonfunctioning tumor that is found incidentally at imaging and ranges from 2 to 17 cm in diameter. Pathologically, a myelolipoma is composed of adipose and hematopoietic tissues. It commonly originates from the adrenal gland and rarely originates from an extra-adrenal location. At imaging, a myelolipoma typically appears as a well-circumscribed mass that contains variable amounts of soft tissue and macroscopic fat (Fig 6). A pseudocapsule has been reported in 75% of cases, with calcification in 24% of cases (8).

Congenital Adrenal Hyperplasia

Congenital adrenal hyperplasia results from 21-hydroxylase deficiency. Prolonged stimulation of the adrenal cortex typically leads to enlarged adrenal glands, occasionally associated with multiple fat-containing adrenal masses (Fig 7). This appearance has been rarely reported in the literature (9,10), although this diagnosis may be underreported because these lesions mimic the appearance of myelolipomas, which seldom exist bilaterally. Chronic adrenocorticotropic hormone and androgen hyperstimulation, with

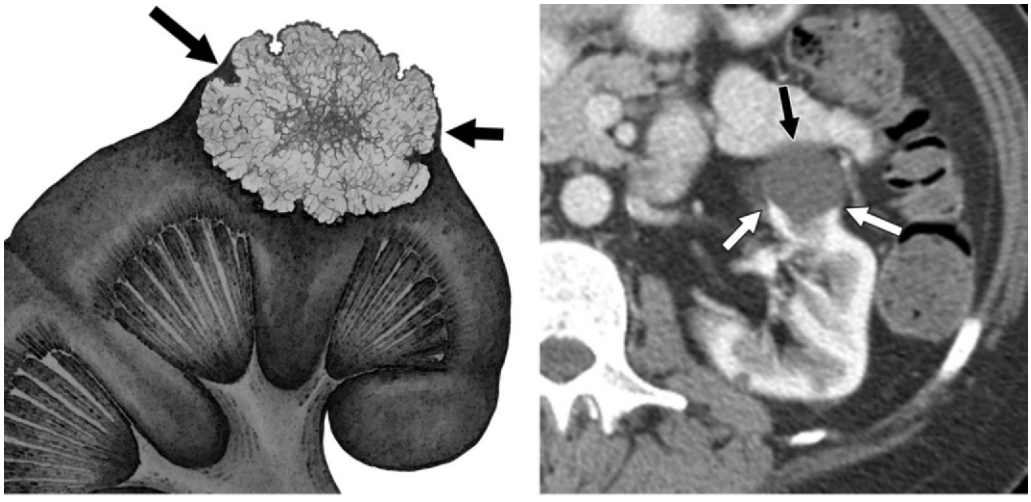

a. b.

Figure 1. Positive beak sign. **(a)** Drawing shows sharp angles (arrows) at the interface of a mass and the kidney. **(b)** Axial contrast-enhanced CT image shows a simple left renal cyst (black arrow) with a sharp beak-shaped interface (white arrows), which implies that the cyst arises from the kidney.

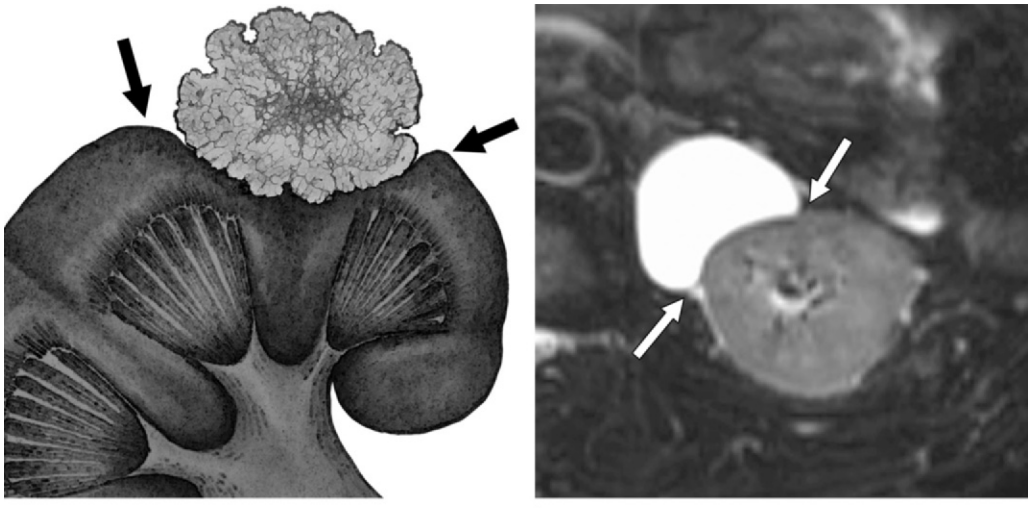

a. b.

Figure 2. Negative beak sign. **(a)** Drawing shows round angles (arrows) at the interface of a mass and the kidney. **(b)** Axial fat-suppressed T2-weighted MR image shows a cystic structure within the perinephric space abutting the renal capsule (arrows). The dull rounded interface between the cystic structure and the kidney indicates that it does not arise from the kidney.

overexpression of their receptors, is assumed to be involved in the pathogenesis of adrenal myelolipomas associated with noncompliant patients with congenital adrenal hyperplasia (11).

Pheochromocytoma

The paraganglionic system is composed of neural crest cells, which are found in the adrenal medulla, parasympathetic ganglia, and chemoreceptors. Tumors that arise from the chromaffin cells of the adrenal medulla are called *pheochromocytomas*, and those that arise in extra-adrenal locations (10%) are referred to as *paragangliomas*. Pheochromocytoma is typically symptomatic, occurring with new-onset paroxysmal, refractory, or recently exacerbated hypertension (12), headache, flushing, and palpitations. Pheochromocytoma has been shown to follow the "rule of 10s," with 10% being malignant, 10% being bilateral, 10% being extra-adrenal, and 10% occurring in children (13). Pheochromocytoma can be associated with multiple endocrine neoplasia, von Hippel–Lindau disease, neurofibromatosis type 1, and nonsyndromic familial pheochromocytoma (14). On contrast-enhanced CT images, pheochromocytomas demonstrate heterogeneous enhancement and thus can have nonspecific imaging manifestations. One-third

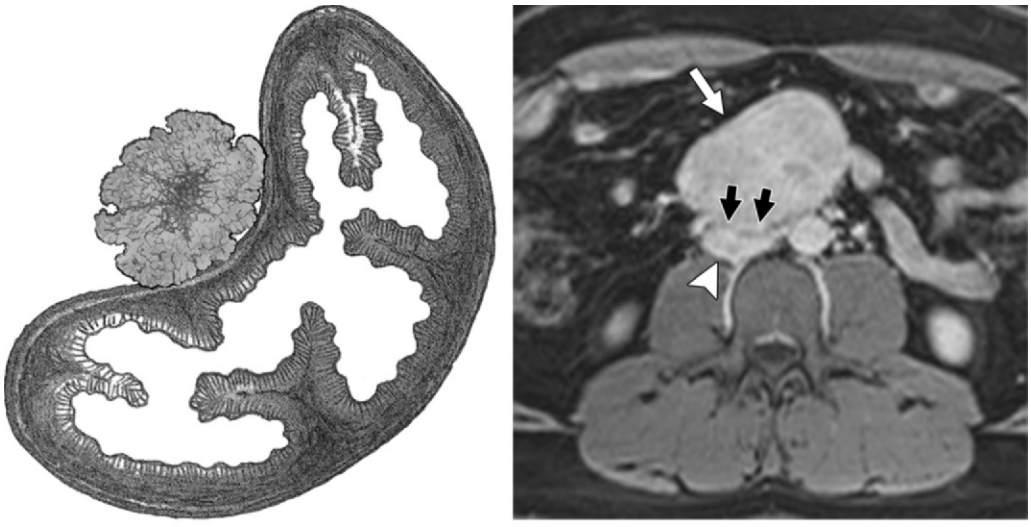

a. b.

Figure 3. Negative embedded organ sign. **(a)** Drawing shows a tumor compressing a hollow viscus organ, which assumes a crescent shape. **(b)** Axial gadolinium-enhanced fat-suppressed T1-weighted MR image shows a primary retroperitoneal paraganglioma (white arrow) compressing the inferior vena cava (arrowhead) and causing it to assume a crescent configuration. The interface of the mass and the inferior vena cava appears smooth and regular (black arrows).

a. b.

Figure 4. Positive embedded organ sign. **(a)** Drawing shows a tumor arising from the wall of a hollow viscus organ, which appears to be embedded in the tumor. **(b)** Coronal contrast-enhanced CT image shows a large homogeneous mass arising from the wall of the terminal ileum. The lumen of the ileum is preserved, and the wall of the ileum appears embedded in the mass at the contact surface (arrows). These findings represent a gastrointestinal stromal tumor of the ileum with a positive embedded organ sign.

of pheochromocytomas mimic lipid-poor adenomas, with an absolute enhancement washout rate of more than 60% and a relative enhancement washout rate of more than 40% (15). On MR images, most cases demonstrate high signal intensity on T2-weighted images, a finding formerly known as the "light bulb sign." However, markedly increased signal intensity on T2-weighted images is not as common as was previously thought. Rarely, microscopic and macroscopic fat can be seen in pheochromocytomas (Fig 8) (16).

Adrenocortical Carcinoma

Although it is the most common adrenal primary malignancy, adrenocortical carcinoma is rare, affecting approximately two patients per million and occurring in patients 30–70 years of age. Adrenocortical carcinoma is an aggressive malignancy with a poor prognosis, although less aggressive forms have been described. Most of these tumors are functional, with approximately 60% of patients experiencing endocrine symptoms typically characterized by Cushing

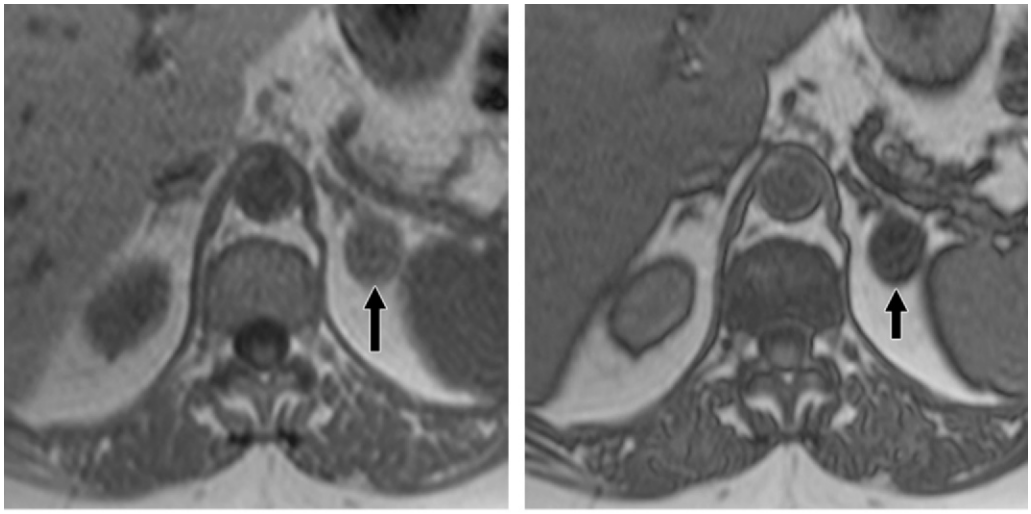

a. b.

Figure 5. Adrenal adenoma in a 43-year-old woman. Axial in-phase **(a)** and opposed-phase **(b)** T1-weighted MR images show a left adrenal mass (arrow). The mass shows signal intensity loss on the opposed-phase image compared with the in-phase image, owing to intracellular fat content.

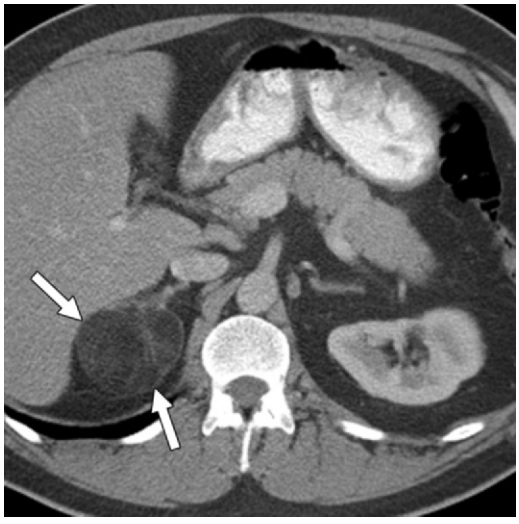

Figure 6. Adrenal myelolipoma in a 45-year-old woman. Axial contrast-enhanced CT image shows a right adrenal mass that contains macroscopic fat (arrows). The mass has higher attenuation than that of retroperitoneal fat because of the myeloid elements.

syndrome (40%) or a mixed hormonal picture of Cushing syndrome and virilization (17). Typically, adrenocortical carcinoma appears as a large mass, usually larger than 6 cm (ranging from 4 to 25 cm in diameter). These tumors typically exhibit heterogeneous contrast enhancement and have absolute and relative contrast material washout rates of less than 60% and less than 40%, respectively. The degree of heterogeneity and large size are more reliable for diagnosis than contrast material washout measurements. Adrenocortical carcinoma has been rarely reported to contain foci of microscopic or macroscopic fat (Fig 9) (18). Fat-containing adrenocortical carcinomas have only a small amount of macroscopic fat relative to the overall lesion size; this may be a helpful clue when determining the diagnosis. Although small myelolipomas may contain small amounts of fat, larger myelolipomas usually contain a substantial amount of fat. Hypertension or evidence of adrenal hormonal excess favors a diagnosis of adrenocortical carcinoma rather than myelolipoma. Myelolipomas can demonstrate enhancement; however, a large heterogeneous mass with substantial peripheral enhancement more likely represents adrenocortical carcinoma than myelolipoma (19).

Adrenal AML

AML is a rare benign mesenchymal tumor that consists of mature adipose tissue, smooth muscle, and blood vessels. AML usually arises from the kidney. The liver is the most common extrarenal location. About 50% of AMLs are associated with tuberous sclerosis. Few cases of AML have been reported to involve the adrenal glands (Fig 10) (14), and the appearance is indistinguishable from that of adrenal myelolipoma.

Adrenal Lipoma

Lipomas are small benign tumors of mesenchymal origin that contain mature fatty tissue and are surrounded by a fibrous capsule; only a few cases have been reported to involve the adrenal glands (20). Adrenal lipoma appears as a well-circumscribed, homogeneous, fatty mass (Fig 11). In contrast to

Figure 7. Congenital adrenal hyperplasia in a 37-year-old woman. Axial contrast-enhanced CT image shows bilateral enlargement of the adrenal glands (black arrows) and multiple fat-attenuating masses (white arrows) in the left adrenal gland.

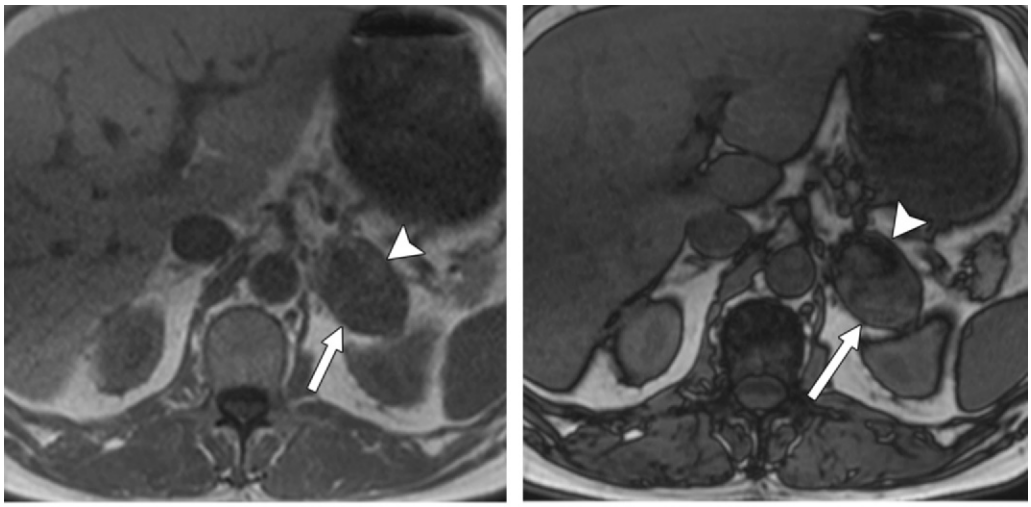

a. **b.**

Figure 8. Adrenal pheochromocytoma in a 57-year-old woman who presented with hypertension. Axial in-phase **(a)** and opposed-phase **(b)** T1-weighted MR images show a left adrenal mass (arrow). The mass displays heterogeneous signal intensity, with a focal area (arrowhead) that shows signal intensity loss on the opposed-phase image compared with the in-phase image due to intracellular fat content.

myelolipomas, no or minimal soft-tissue attenuation should be visualized within the lesion.

Management of Fat-containing Adrenal Lesions

Clinical and imaging features that help differentiate fat-containing adrenal lesions are listed in Table 3. Most benign adrenal tumors are adrenal cortical adenomas that contain varying amounts of intracytoplasmic lipid and can be diagnosed on the basis of a combination of imaging features. Myelolipomas and AMLs are usually predominantly fatty masses. Most small, nonfunctioning, benign adrenal lesions (adenomas, myelolipomas, lipomas, and AMLs) are managed conservatively. Adrenalectomy is indicated for any biochemically functioning tumor and for large or symptomatic tumors. Predominantly soft-tissue masses that contain a small amount of macroscopic fat are usually adrenocortical carcinomas or pheochromocytomas, and both require surgical resection.

Fat-containing Renal Lesions

Renal AML

Renal AML is the most common benign mesenchymal tumor of the kidney. Pathologically, it is composed of fat, smooth muscle, and abnormal blood vessels. AML may be sporadic or occur in association with tuberous sclerosis. The sporadic form accounts for 80%–90% of cases and is most common in middle-aged women (21). Most cases are readily diagnosed because of the predominant macroscopic fat content.

Thin-section CT is preferred for diagnosing AML when there are small amounts of fat (22).

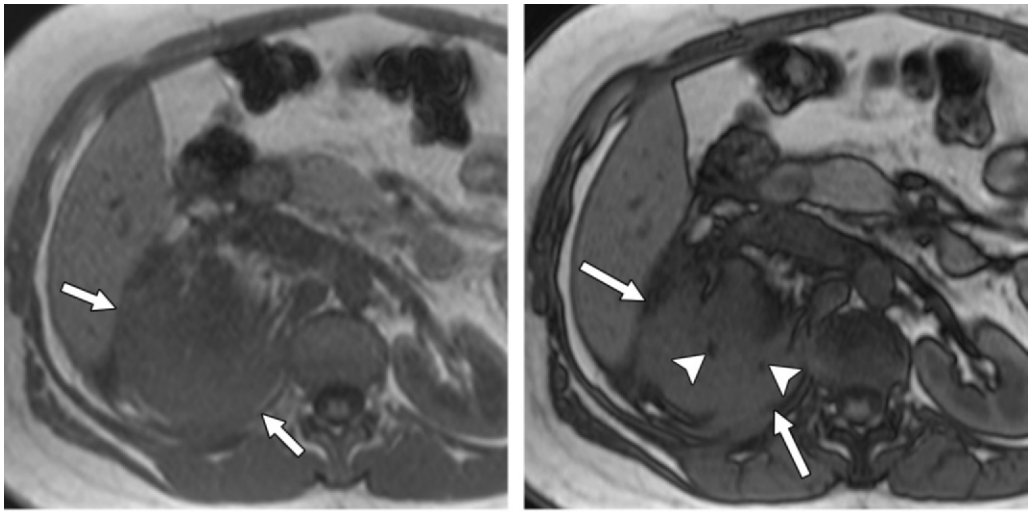

a. b.

Figure 9. Adrenocortical carcinoma in a 53-year-old man. Axial in-phase **(a)** and opposed-phase **(b)** T1-weighted MR images show a right adrenal mass (arrows). Foci of signal intensity loss seen on the opposed-phase image (arrowheads) are due to intracellular fat content.

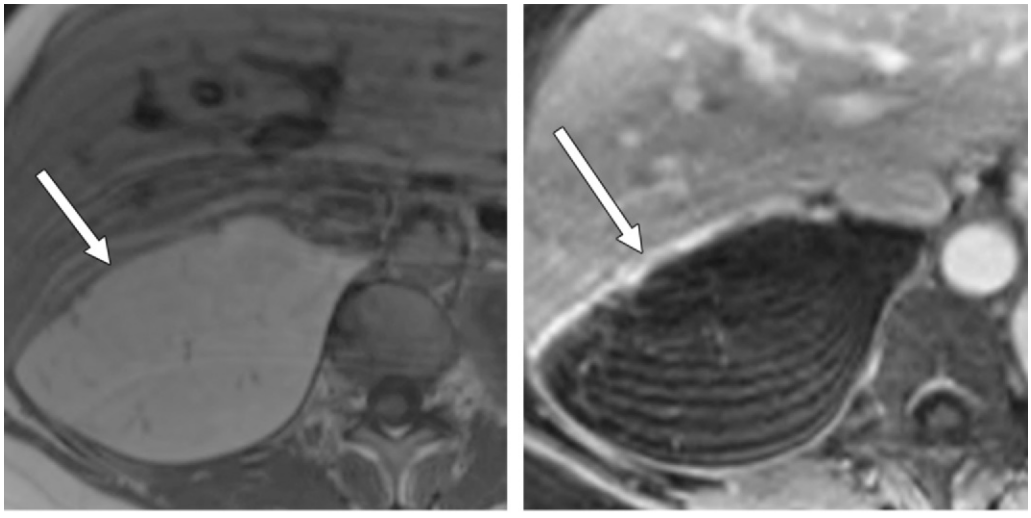

a. b.

Figure 10. Adrenal AML in a 49-year-old woman. Axial nonenhanced **(a)** and fat-suppressed gadolinium-enhanced **(b)** T1-weighted MR images show a right adrenal mass (arrow). The mass shows high T1 signal intensity, with signal intensity loss seen on the fat-suppressed T1-weighted image. There is a thin peripherally enhancing capsule and minimal enhancement of the fatty tumor.

Loss of signal intensity on gradient-echo or spin-echo MR images acquired with fat suppression is diagnostic of AML; at chemical shift MR imaging, detection of "India ink" artifact at fat-water interfaces is also highly suggestive of AML (23).

AMLs with minimal fat are tumors in which intratumoral fat cannot be visualized on CT images and are characterized by a predominance of blood vessels, muscle, or immature fat or a scattering of a small amount of fat within other components (24). There is substantial overlap between CT and MR imaging findings of *(a)* AML with minimal fat and *(b)* RCC, with conflicting data on the ability of imaging to allow differentiation between the two conditions (25,26). AMLs with minimal fat are usually hyperattenuating relative to the renal parenchyma on nonenhanced CT images and hypointense on T2-weighted MR images, inherent features that reflect the predominant smooth muscle component and classically overlap with features of papillary RCC (27). Findings suggestive of the diagnosis of AML without visible fat include an angular interface between the mass and the underlying normal renal parenchyma, a low-attenuation rim at the periphery of the mass on nonenhanced CT images, homogeneous attenuation, absence of calcification, and presence of other lesions with

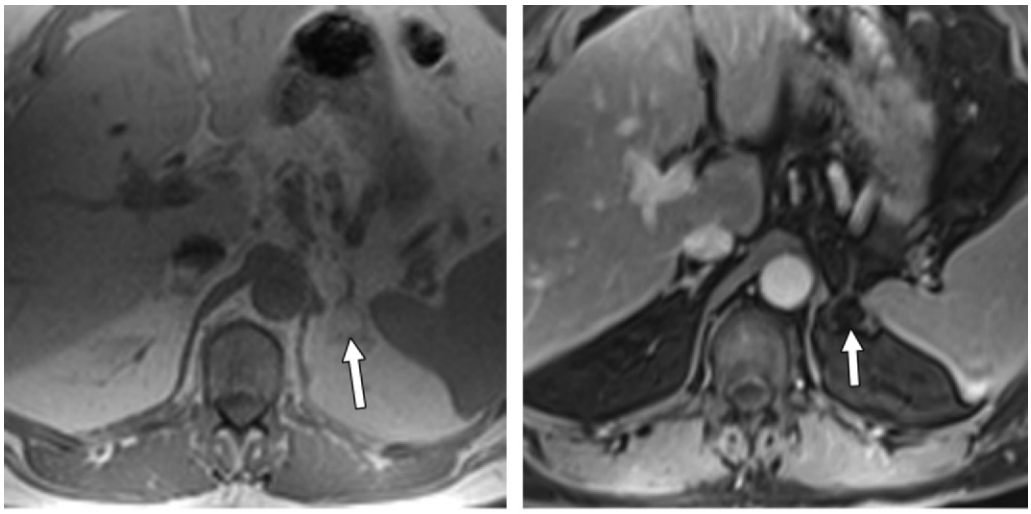

a. b.

Figure 11. Adrenal lipoma in a 47-year-old woman. Axial in-phase **(a)** and gadolinium-enhanced fat-suppressed volumetric interpolated breath-hold (VIBE) **(b)** T1-weighted MR images show a left adrenal mass (arrow). The mass has homogeneous high signal intensity in **a** and low signal intensity in **b**, with no appreciable enhancement.

Table 3: Differential Diagnosis of Fat-containing Adrenal Lesions

Parameter	Adrenal Adenoma	Adrenal Myelolipoma	Pheochromocytoma	Adrenocortical Carcinoma	Adrenal AML	Adrenal Lipoma
Incidence	Common	Common	Not uncommon	Rare	Rare	Rare
Likelihood of presence of fat	Common	Common	Rare	Rare	Common	Common
Fat quantity	Microscopic fat	Predominantly fatty lesion	Microscopic or small amount of macroscopic fat in a predominantly soft-tissue mass	Microscopic or small amount of macroscopic fat in a predominantly soft-tissue mass	Predominantly fatty lesion	Predominantly fatty lesion
Clinical syndrome	Primary aldosteronism or Cushing syndrome	None	Symptoms of catecholamine excess	Cushing syndrome with or without virilization; primary aldosteronism	None	None
Calcifications	Possible	Possible	Possible	Possible	Absent	Absent
Texture	Homogeneous	Heterogeneous	Heterogeneous	Heterogeneous	Homogeneous or heterogeneous	Homogeneous
Associated conditions	Familial adenomatous polyposis	Congenital adrenal hyperplasia	MEN, VHL, NF1, and nonsyndromic familial pheochromocytoma	None	Tuberous sclerosis	None

Note.—MEN = multiple endocrine neoplasia, NF1 = neurofibromatosis type 1, VHL = von Hippel–Lindau disease.

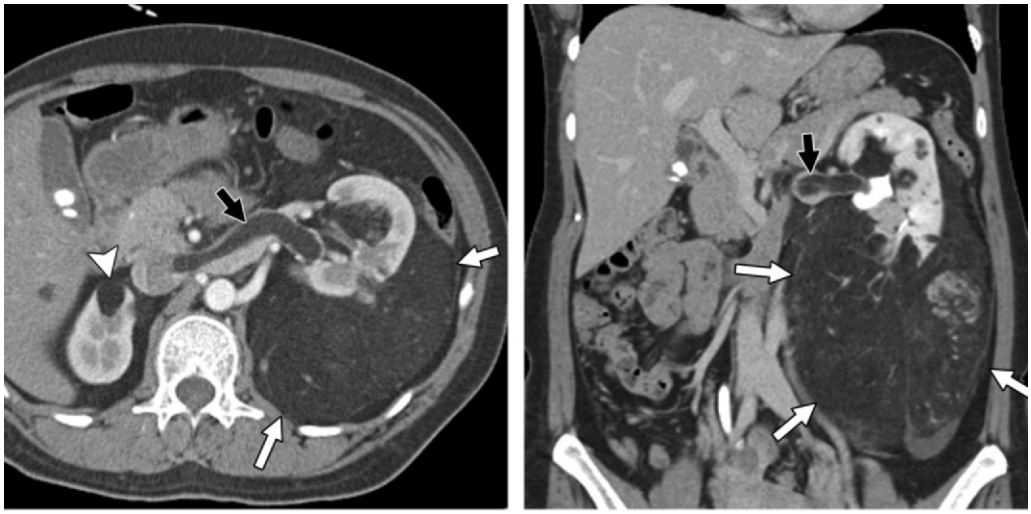

a. b.

Figure 12. Renal AML in a 48-year-old woman with a history of tuberous sclerosis. Axial **(a)** and coronal **(b)** contrast-enhanced CT images show a left renal fat-containing mass (white arrows). Note the fatty tumor thrombus in the left renal vein (black arrow). A fat-containing lesion is also seen in the right kidney (arrowhead in **a**).

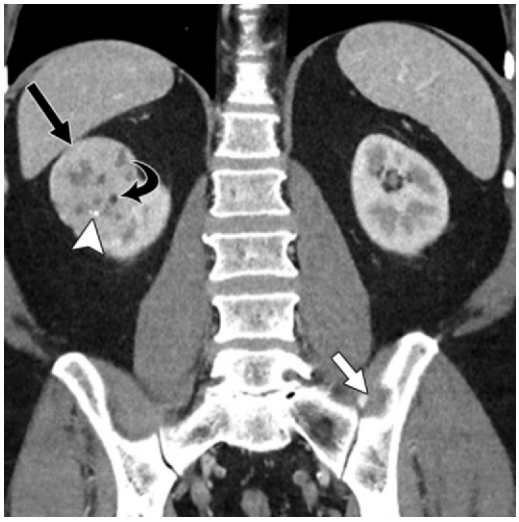

Figure 13. RCC in a 56-year-old man. Coronal contrast-enhanced CT image shows an enhancing right renal mass (straight black arrow). The mass has soft-tissue attenuation, with small foci of calcifications (arrowhead) and fat attenuation (curved black arrow). A metastatic lytic lesion of the left iliac bone (white arrow) is also seen.

classic imaging features of AML (28). Calcification within an AML is exceedingly rare; only six cases of AMLs that contained calcification have been reported in the literature to date (29).

Invasion of the renal vein is a rare but recognized complication of benign AML, and it does not imply malignancy or metastasis (Fig 12). Contributing factors to development of renal vein invasion include large size and central location of the AML (21).

Differentiating an exophytic AML from a perinephric liposarcoma can occasionally be difficult, as both conditions appear as a fatty mass within the perinephric space. Features that strongly favor an exophytic AML are renal cortical tumoral vessels (neovascularity) or a renal parenchymal defect, usually with an angular interface with the normal renal parenchyma at the site of tumor contact, whereas tumoral calcifications are suggestive of a perinephric liposarcoma (30).

Renal Cell Carcinoma

The presence of fat within an RCC is a rare phenomenon. It denotes fatty marrow elements in the setting of osseous metaplasia, perinephric or renal sinus fat engulfed by the tumor, or cholesterol necrosis (31). Fat has been reported at pathologic examination of nephrectomy specimens in about 0.24% of cases of RCC, mostly in the clear cell type, with fat foci ranging from 0.1 to 1.8 cm in diameter (32).

All reported cases of fat-containing RCC contain small foci of fat scattered within a soft-tissue mass (33–35) and can be readily differentiated from classic AML, which usually contains abundant macroscopic fat. Most fat-containing RCCs contain calcifications in close proximity to fat foci (Fig 13). RCCs that contain fat without calcifications are extremely rare (Fig 14) (36).

Because of the smooth muscle content, AMLs with minimal fat are typically hypointense on T2-weighted MR images and can be readily differentiated from clear cell RCCs, which are typically hyperintense on T2-weighted images. Therefore, an enhancing renal mass that is hypoattenuating on nonenhanced CT images and hyperintense

Figure 14. RCC in a 63-year-old man. Coronal contrast-enhanced CT image shows an enhancing right renal mass (black arrow) with soft-tissue attenuation, small foci of fat attenuation (white arrow), and no visible calcifications.

Figure 15. Renal lipoma in a 45-year-old woman. Axial nonenhanced CT image shows a homogeneous, well-circumscribed, fat-attenuating right renal mass (arrow).

Figure 16. Renal liposarcoma in a 65-year-old man. Axial contrast-enhanced CT image shows a fat-attenuating lesion in the left kidney (arrows). The lesion extends from the renal sinus to the perinephric fat and is centered on the renal capsule. Pathologic examination demonstrated a well-differentiated liposarcoma arising from the renal capsule.

on T2-weighted MR images is more likely to be an RCC than an AML with minimal fat. On the other hand, papillary RCCs are also typically hypointense on T2-weighted MR images and hyperattenuating on nonenhanced CT images. Therefore, a homogeneously enhancing renal mass that is hyperattenuating on nonenhanced CT images and hypointense on T2-weighted MR images could represent an AML with minimal fat or a papillary RCC. Percutaneous biopsy is the only way to distinguish between these two entities, short of surgical resection (37,38). It should be noted that fat-containing oncocytomas have also been reported (31).

Renal Lipoma and Liposarcoma

Primary intrarenal lipomas are extremely rare mesenchymal neoplasms that typically arise from the renal capsule. Intrarenal lipomas are more common in middle-aged women (39) but can be seen even in young children (40). Small intrarenal lipomas are asymptomatic, but large tumors may manifest with abdominal pain.

At imaging, renal lipoma appears as a well-circumscribed homogeneous mass that is almost exclusively composed of macroscopic fat (Fig 15). A soft-tissue component and feeding vessels are rarely seen (41).

Renal liposarcoma is a rare tumor, with only a few documented cases in the literature (42). It arises from either the renal sinus or the capsule, and in large tumors it may be difficult to determine the origin of the tumor (Fig 16) (42). The imaging appearance of liposarcoma varies, depending on the tumor grade. Well-differentiated liposarcomas are indistinguishable from lipomas and appear as well-defined predominantly fat-containing lesions with minimal soft-tissue attenuation. Poorly differentiated tumors, however, appear as locally invasive predominantly soft-tissue masses with variable amounts of fat.

Renal Replacement Lipomatosis

Renal replacement lipomatosis is a rare benign pathologic entity in which marked atrophy of the renal parenchyma is accompanied by extensive fibrofatty proliferation of the renal sinus and perinephric space (Fig 17) (43). The condition is

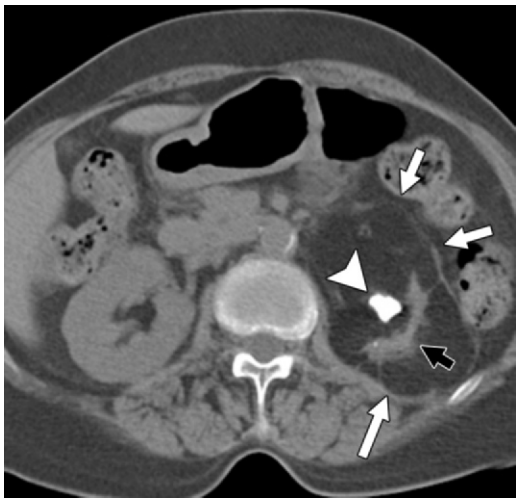

Figure 17. Renal replacement lipomatosis in a 47-year-old woman. Axial nonenhanced CT image shows marked thinning of the left kidney (black arrow), a renal pelvis stone (arrowhead), and expansion of perinephric fat (white arrows).

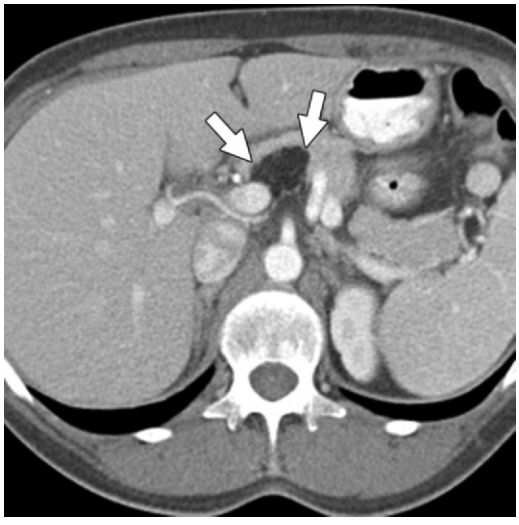

Figure 18. Pancreatic lipoma in a 62-year-old woman. Axial contrast-enhanced CT image shows a well-circumscribed homogeneous fat-attenuating mass (arrows) in the pancreatic body.

usually unilateral and may be segmental. In most cases, it is secondary to calculus disease, resulting in hydronephrosis and chronic inflammation (43). Renal replacement lipomatosis can be differentiated from fat-containing neoplasms that arise from the renal parenchyma, renal sinus, renal capsule, or perinephric space by diffuse uniform distribution of fat within the renal sinus and perinephric space, marked loss of renal parenchyma, loss of renal function, and renal calculi.

Management of Fat-containing Renal Lesions

A predominantly fatty renal mass is almost always an AML. Small (<4-cm) AMLs have traditionally been managed conservatively because of the absence of malignant potential and a low propensity for hemorrhage, but follow-up is recommended to assess growth. Symptomatic tumors or tumors larger than 4 cm can be selectively embolized or resected with partial or radical nephrectomy (44). Other lesions with large fatty components include lipoma and liposarcoma. Differentiating renal lipoma or well-differentiated liposarcoma from AML may be difficult: AMLs may contain large aneurysmal vessels, while lipomas and liposarcomas are relatively avascular and rarely occur with multiple lesions, as may be seen with AMLs. Biopsy is usually required in a large lesion; however, surveillance may be adequate for small purely fatty lesions. Poorly differentiated liposarcoma is more invasive and contains a variable amount of soft-tissue elements.

Fat-containing RCC may contain subtle sparse areas of fat within a predominantly soft-tissue mass and can be readily differentiated from classic AML, which usually contains an abundant amount of fat. The main differential diagnostic consideration for fat-containing RCC is AML with minimal fat. The latter is almost always small (≤3 cm) and lacks the calcifications commonly seen with RCC (34).

Fat-containing Pancreatic Lesions

Pancreatic Lipoma

Pancreatic lipomas are likely underreported in the literature. Gossner (45) identified six pancreatic lipomas in a sample of 100 consecutive abdominal CT examinations. Lipomas are usually incidentally found during abdominal imaging and are more common in the pancreatic head. Pancreatic lipomas are rarely symptomatic, although they may result in abdominal pain and obstruction of pancreatic and biliary ducts (45).

At imaging, pancreatic lipomas appear as well-circumscribed homogeneous masses with a sharp interface with the normal pancreatic parenchyma (Fig 18). Calcifications are characteristically absent in pancreatic lipomas.

A large (>5-cm) fatty pancreatic mass with irregular borders, evidence of infiltration of adjacent structures, and areas of soft-tissue attenuation should raise suspicion for pancreatic liposarcoma; further evaluation is indicated in such cases.

Pancreatic Mature Cystic Teratoma

Pancreatic teratomas represent a rare entity, with fewer than 50 cases described in the world literature. The mean age of reported patients is 36.4 years (age range, 4 months to 74 years) (46). Most pancreatic teratomas are found in the head

and/or body of the gland and are symptomatic, commonly occurring with abdominal or back pain. The imaging appearance of pancreatic teratomas is the same as that of teratomas elsewhere, with a heterogeneous appearance due to multiple tissue components. They usually appear as fatty and/or cystic masses with fat-fluid levels. Coarse calcifications are usually present, with or without soft-tissue components (Fig 19), which help differentiate mature cystic teratoma from the more common pancreatic lipoma (47). The echogenicity of pancreatic teratomas varies on abdominal or endoscopic US images, ranging from hypoechoic (46,48) to hyperechoic (47) findings relative to the normal underlying pancreatic parenchyma.

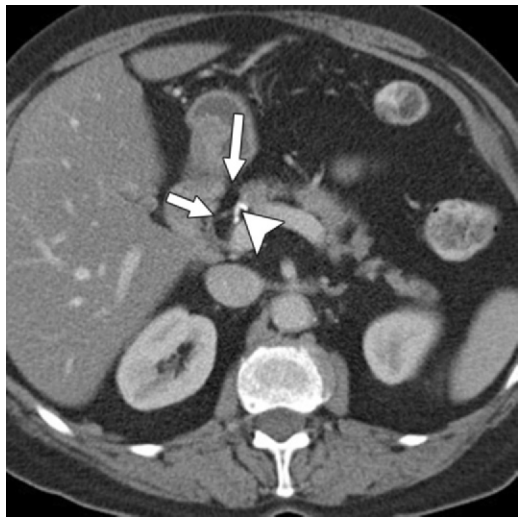

Figure 19. Pancreatic mature cystic teratoma in a 33-year-old woman. Axial contrast-enhanced CT image shows a well-circumscribed homogeneous fat-attenuating mass (arrows) in the pancreatic head. Nodular calcification (arrowhead) is seen at the periphery of the fatty mass.

Pancreatic Lipomatosis

Pancreatic lipomatosis, or fatty replacement of the pancreas, is the most common pathologic finding in the adult pancreas. It can be focal or diffuse, and in some instances, it can mimic a pancreatic mass (49). Complete replacement of the pancreas by fat is seen most commonly in patients with cystic fibrosis or, occasionally, in rare conditions such as Shwachman-Diamond syndrome or Johanson-Blizzard syndrome. In adult patients with cystic fibrosis, complete fatty replacement is the most common pancreatic finding on images (Fig 20), with a reported prevalence of 51%–75%; it is most commonly identified in older patients (50). Pancreatic calcifications occur in roughly 7% of patients with cystic fibrosis and are usually found along the course of the pancreatic duct. Pancreatic cysts are relatively common in patients with cystic fibrosis and probably occur secondary to duct obstruction by inspissated secretions. Cysts are usually small, measuring 1–3 mm, and are best demonstrated on T2-weighted MR images or MR cholangiopancreatographic images (50,51). A gland that is markedly enlarged with fatty replacement has been termed *lipomatous pseudohypertrophy of the pancreas* (Fig 20). Lesser degrees of diffuse fatty replacement are more common in patients with diabetes, metabolic syndrome, steroid use, chronic pancreatitis, or obesity and in the elderly.

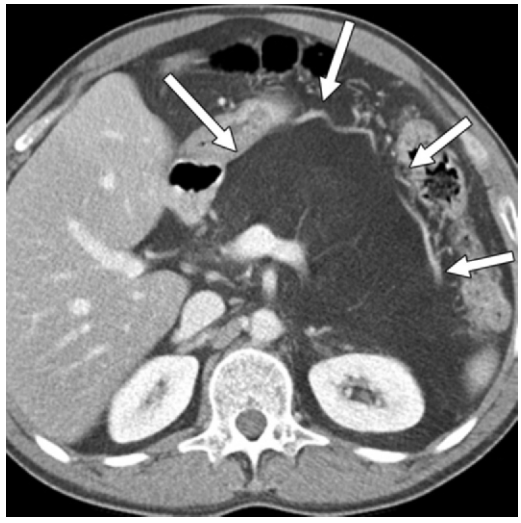

Figure 20. Pancreatic lipomatosis in a 23-year-old man with cystic fibrosis. Axial contrast-enhanced CT image shows expansion and complete replacement of the pancreas with lipomatous tissue (arrows).

Fatty replacement of the pancreas can be focal and may resemble a pancreatic mass (Fig 21); it typically involves the anterior head, with sparing of the posterior head and the uncinate process (52). It is postulated to be secondary to the different histologic characteristics of the ventral and dorsal pancreatic anlages and may demonstrate mass effect and contrast enhancement due to entrapped normal parenchymal tissue. Nonenhanced CT is usually adequate for depicting the negative attenuation values of a focal pancreatic lesion and to confirm its fatty nature. However, a mild degree of focal fatty change in the pancreas can be difficult to diagnose with CT alone because the attenuation values may be in the range of fluid attenuation values. Areas of focal fatty replacement may show contrast enhancement on CT images because of enhancement of normal pancreatic parenchyma entrapped between fatty replaced parenchyma. Chemical shift MR imaging is diagnostic for confirming focal fatty change in the pancreas by demonstrating signal intensity loss on opposed-phase images when compared with in-phase images (49).

Figure 21. Focal fatty replacement of the pancreatic head in a 67-year-old woman. Axial contrast-enhanced CT image shows a fat-attenuating masslike structure replacing the pancreatic head (arrows). The mass appears heterogeneous and has a lacy appearance due to normal pancreatic parenchyma intermixed with fat.

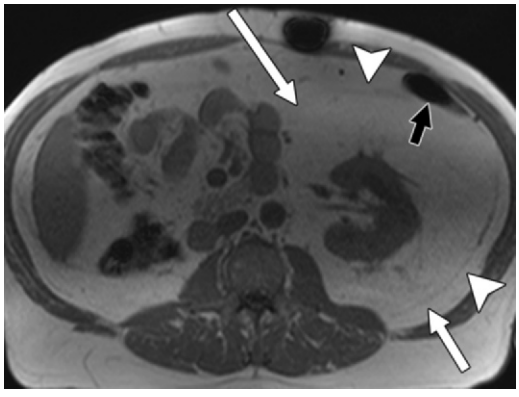

Figure 22. Retroperitoneal lipomatosis in a 57-year-old man. Axial T1-weighted MR image shows marked accumulation of fat in the left perinephric space (white arrows), with distension of the renal fascia (arrowheads) and anterior displacement of the descending colon (black arrow). The patient underwent a right nephrectomy for RCC and was found to have perinephric lipomatosis.

Management of Fat-containing Pancreatic Lesions

Pancreatic lipomatosis is a diffuse process that involves the entire pancreas and is easily diagnosed at imaging. Focal pancreatic lesions include lipoma, liposarcoma, mature cystic teratoma, and focal fatty replacement. Lipoma is well circumscribed and homogeneous, features that help to differentiate it from focal fatty replacement. The presence of fat-fluid levels and coarse calcifications, with or without soft-tissue components, can differentiate pancreatic mature cystic teratoma from pancreatic lipoma. Differentiation of fat-containing pancreatic lesions does not have clinical significance, as none of these lesions require intervention or treatment. The most important issue in these cases is that the presence of fat helps to exclude the diagnoses of adenocarcinoma and neuroendocrine tumors, which are not known to contain fatty elements. The only exception for a fat-containing pancreatic mass that requires intervention is the rare pancreatic liposarcoma. Those tumors are usually large and heterogeneous and contain soft-tissue elements together with fatty components, and biopsy or surgical excision is required in such cases.

Fat-containing Primary Retroperitoneal Lesions

Nonneoplastic Lesions

Retroperitoneal Lipomatosis.—Lipomatosis is a benign metaplastic overgrowth of mature unencapsulated white fat. The condition usually affects the extraperitoneal pelvis and less commonly affects the abdominal retroperitoneum—specifically the perinephric space. The patient may be asymptomatic or may present with nonspecific symptoms related to organ compression, including abdominal pain and urinary or gastrointestinal symptoms. Lipomatosis is more common in men (with a ratio of men to women of 18:1), particularly African-American men, with a mean age of 48 years. There is no statistically significant association with obesity (53). CT and MR images show expansion of the pelvic or retroperitoneal fat, with mass effect on the pelvic and abdominal structures pushing the bowel loops anteriorly and compressing the urinary bladder, resulting in a "pear-shaped" bladder (Fig 22). A few fibrous tissue strands may be present, but there is no enhancing soft-tissue component. The ureters may be displaced medially, and the femoral veins may be stretched (54).

Human Immunodeficiency Virus–related Lipodystrophy.—Long-term use of antiretroviral therapy in patients with human immunodeficiency virus or acquired immunodeficiency syndrome is associated with disturbances of adipose tissue distribution, accompanied by metabolic and endocrine disorders, collectively referred to as *antiretroviral therapy–associated lipodystrophy syndrome*. In this syndrome, clinical conditions are grouped together that describe changes in body fat distribution, including lipoatrophy and/or lipoaccumulation. Lipoatrophy is related to subcutaneous fat loss and typically involves the limbs (predominance of lower limbs), face, and buttocks. Lipohypertrophy consists of the accumulation of

adipose tissue and usually involves the retroperitoneum, breast, anterior neck, and dorsocervical ("buffalo hump") regions (55). At imaging, it resembles retroperitoneal lipomatosis, with a notable paucity of subcutaneous fat (Fig 23).

Retroperitoneal Panniculitis.—Mesenteric panniculitis is an inflammatory process of the mesenteric fat. It is a rare condition characterized by chronic mesenteric inflammation, likely an immunoglobulin G4–related sclerosing condition. It usually involves the mesentery of the small bowel, especially at its root, but occasionally it involves the mesocolon, peripancreatic region, omentum, retroperitoneum, or pelvis. It is characterized by an infiltration of lipid-laden macrophages and is associated with variable degrees of inflammation and fibrosis (56). The CT appearance varies from subtle increased attenuation of the mesenteric and retroperitoneal fat to a solid soft-tissue mass. Preservation of fat around the mesenteric vessels ("fat ring sign") and a tumoral pseudocapsule have been described in patients with mesenteric panniculitis (Fig 24) (57). Retroperitoneal involvement can be differentiated from other conditions involving the retroperitoneal fat by the typical coexisting involvement of the mesentery.

Retroperitoneal Fat Necrosis.—Retroperitoneal fat necrosis is usually caused by the lipolytic effect of pancreatic enzymes released during acute pancreatitis. It usually is accompanied by pancreatic parenchymal necrosis but can occur without visible pancreatic involvement (58). On CT images, the involved retroperitoneal fat shows increased attenuation, more than that of normal retroperitoneal fat, with scattered nodules and thick septa. The process may extend into the various retroperitoneal compartments, the small bowel mesentery, and the transverse mesocolon. The process may traverse the strong perinephric fascia to involve the perinephric compartment (59). A clinical history of a prior episode of acute pancreatitis is usually helpful in establishing the diagnosis. Other causes of retroperitoneal fat necrosis have been reported, including long-term use of steroids (Fig 25) (60).

Encapsulated Fat Necrosis.—Encapsulated fat necrosis is a degenerative process that involves mature adipose tissues and is much more common in the breasts and extremities. It is thought to result from a traumatic or ischemic insult that causes fat degeneration; however, the exact pathogenesis is unknown. Its imaging appearance may be complex; fat-attenuation lesions contain linear or masslike fluid or show soft-tissue attenuation and are surrounded by a thick capsule. The capsule may weakly enhance after administration of contrast material and can calcify in chronic lesions. There is no local invasion and only minimal mass effect on surrounding structures. The size and appearance can change over time. A fat-fluid level may be seen in areas of fat necrosis (Fig 26) (61). On MR images, encapsulated fat necrosis usually appears heterogeneous on both T1- and T2-weighted images, with areas of high and low signal intensity; inhomogeneous enhancement is seen after

Figure 23. Human immunodeficiency virus–related lipodystrophy in a 44-year-old man. Coronal contrast-enhanced CT image shows marked bilateral expansion of the perinephric spaces (arrows) and a notable paucity of subcutaneous fat.

Figure 24. Mesenteric and retroperitoneal panniculitis in a 44-year-old man. Axial nonenhanced CT image shows typical subtle increased attenuation in the mesentery and retroperitoneal fat of the left renal sinus and around the aorta. There is preservation of fat surrounding the mesenteric vessels (arrowheads). A thin band of soft-tissue attenuation (arrows) separates the abnormal mesentery from the surrounding normal fat.

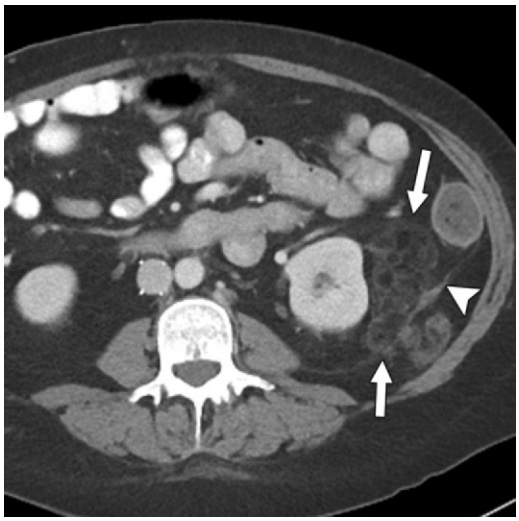

Figure 25. Retroperitoneal fat necrosis in a 45-year-old woman who was treated with steroids and warfarin for ulcerative colitis and pulmonary emboli, respectively. Axial contrast-enhanced CT image shows an ill-defined, hazy, fat- and soft-tissue–attenuation lesion (arrows) centered in the left perinephric space and crossing the posterior renal fascia (arrowhead) into the posterior pararenal space. The patient had undergone mastectomy a few years earlier for massive breast fat necrosis.

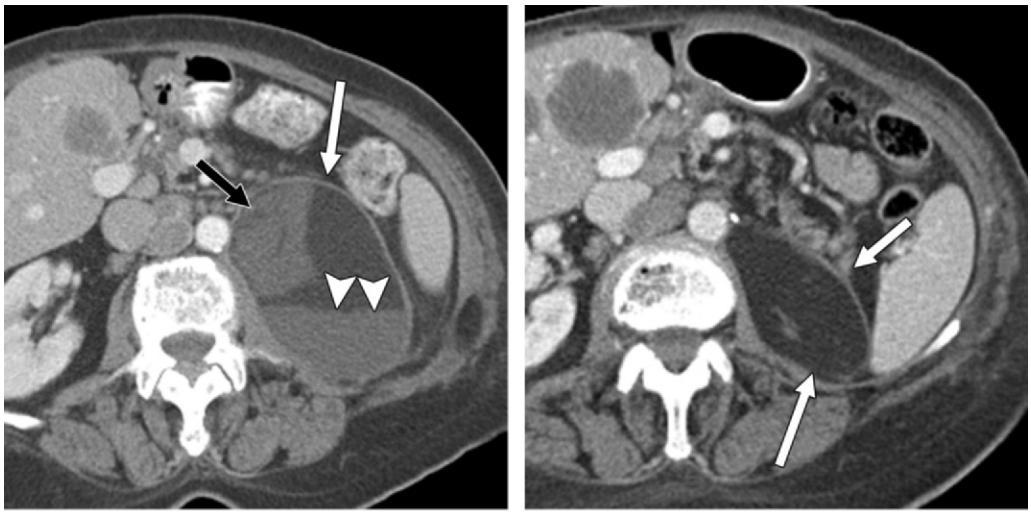

a. **b.**

Figure 26. Encapsulated fat necrosis in a 75-year-old woman who underwent a radical nephrectomy for RCC. **(a)** Axial contrast-enhanced CT image obtained 5 months after surgery shows a well-circumscribed cystic lesion (white arrow) in the nephrectomy bed. The lesion has a well-defined capsule, a fat-fluid level (arrowheads), and a nondependent soft-tissue component (black arrow). **(b)** Axial contrast-enhanced CT image obtained 7 months later shows an interval decrease in the size of the fatty mass (arrows) and resolution of the fluid and soft-tissue components.

intravenous gadolinium-based contrast material administration. A peripheral rim of low signal intensity on both T1- and T2-weighted images has been described and corresponds to the fibrotic peripheral capsule (62).

Differentiating encapsulated fat necrosis from liposarcoma can be challenging. Patients with encapsulated fat necrosis usually have a documented history of surgery or trauma. Encapsulated fat necrosis is well circumscribed and has a surrounding capsule, whereas liposarcoma is usually less defined, lacks a capsule, and may invade surrounding structures. Encapsulated fat necrosis tends to decrease in size over time, whereas liposarcoma tends to progressively increase in size (63).

Neoplastic Lesions

Tumors of Adipose Origin

Lipoma is a benign mesenchymal tumor composed of mature adipose tissue, whereas liposarcoma is its malignant counterpart. These tumors can be encountered virtually anywhere in the body at any age. Retroperitoneal liposarcomas can be asymptomatic for a long period and commonly occur in older patients (in the 5th–7th decades of life). At CT, lipomas appear as well-defined homogeneous masses with fat attenuation. Areas of soft-tissue attenuation may be seen within the tumor and may represent fat necrosis, septa, or normal adjacent structures. However, the presence of a predominantly solid soft-tissue

component or adjacent organ invasion should raise suspicion for liposarcoma. Retroperitoneal liposarcomas are classified into five groups: well-differentiated liposarcoma, myxoid liposarcoma, round cell liposarcoma, pleomorphic liposarcoma, and dedifferentiated liposarcoma. The imaging appearance of liposarcoma varies, depending on the tumor group. Well-differentiated liposarcomas appear as well-defined predominantly fat-containing lesions with minimal soft-tissue attenuation (Fig 27) and commonly contain thin septa. The appearance may be indistinguishable from lipoma, and any retroperitoneal purely fatty lesion should be considered a well-differentiated liposarcoma rather than a lipoma until proven otherwise with histologic examination (64,65). Because dedifferentiation always occurs within a well-differentiated liposarcoma, a dedifferentiated liposarcoma appears identical to a well-differentiated liposarcoma, and dedifferentiation is suggested by focal nodular nonlipomatous regions larger than 1 cm (Fig 28) (66). At CT, myxoid liposarcomas typically have lower attenuation than adjacent muscle but higher attenuation than simple fluid. They demonstrate low signal intensity on T1-weighted images and high signal intensity on T2-weighted images and resemble cysts because of the large amounts of extracellular myxoid material. However, areas of high signal intensity on T2-weighted images do enhance after contrast material administration (Fig 29). Most myxoid liposarcomas have enough fat to suggest the diagnosis of liposarcoma. Thick septa and patchy or nodular soft-tissue components are commonly seen. Round cell liposarcoma and pleomorphic liposarcoma exhibit soft-tissue tumor attenuation and signal intensity with a minimal amount of fat (Fig 30) (66).

In an infant or child, the most likely diagnosis for a well-circumscribed fat-containing lesion is lipoblastoma. Poorly circumscribed lesions with an infiltrative growth pattern are described as lipoblastomatosis. Most patients develop lipoblastoma before the age of 3 years; however, the diagnosis has been assigned in newborns and in patients as old as 16 years of age. The main feature of retroperitoneal lipoblastoma is the presence of fat. However, the amount of fat varies, depending on the cellular composition of the lesion and the presence of myxoid material (Fig 31). Calcifications are rare. Lipoblastomas tend to be encapsulated with internal septa, whereas lipoblastomatosis is unencapsulated and shows signs of infiltration of surrounding structures (64,67).

A hibernoma is a rare benign tumor that contains immature fat cells (brown fat), which are commonly found in large quantities in hibernating animals. On US images, hibernomas are echogenic and may have well-defined or ill-defined borders. Increased blood flow in large vessels on the surface of a hibernoma may be visualized at Doppler US. On CT images, hibernomas appear as fat-attenuating lesions, with attenuation slightly higher than that of subcutaneous fat. They usually contain enhancing soft-tissue septa, and calcifications are notably absent. Their appearance can be heterogeneous because they contain variable amounts of brown and white fat, myxoid material, and spindle cell elements. The presence of a large branching vessel within a fatty-appearing lesion is strongly suggestive of hibernoma (68). On MR images, most hibernomas are slightly hypointense relative to subcutaneous fat on T1-weighted images and demonstrate

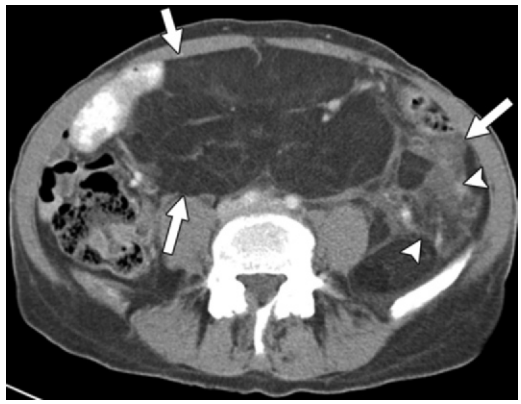

Figure 27. Retroperitoneal well-differentiated liposarcoma in a 54-year-old woman. Axial contrast-enhanced CT image shows a retroperitoneal mass (arrows) with fat attenuation and areas of soft-tissue attenuation (arrowheads). Pathologic analysis demonstrated well-differentiated sclerosing liposarcoma.

Figure 28. Perinephric dedifferentiated liposarcoma in a 52-year-old man. Axial contrast-enhanced CT image shows a mass (arrows) in the left perinephric space. The mass has fat attenuation and multiple lobules of soft-tissue attenuation (arrowheads).

a. b.

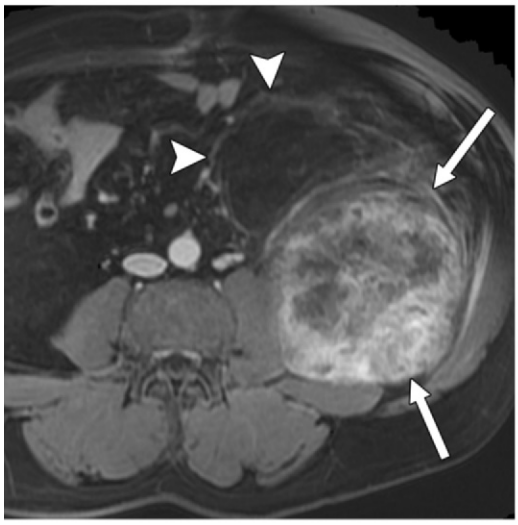

c.

Figure 29. Myxoid liposarcoma in a 63-year-old man. Coronal T2-weighted MR image **(a)**, axial fat-suppressed T1-weighted MR image **(b)**, and axial gadolinium-enhanced fat-suppressed T1-weighted MR image **(c)** show a mass in the left posterior pararenal space (arrows). The mass demonstrates high signal intensity in **a** and low signal intensity in **b** and enhances avidly after gadolinium-based contrast material administration. Note the displacement of the inferior aspect of the left perinephric space (arrowheads in **b** and **c**).

variable signal intensity on T2-weighted images, owing to their variable tissue contents. Less commonly, they demonstrate signal intensity that parallels that of subcutaneous fat. Contrast enhancement varies from none to intense and from focal to diffuse. Positron emission tomography with fluorine 18 fluorodeoxyglucose (FDG) has the potential to allow differentiation of hibernomas from other fat-containing lesions because of the presence of brown fat, which has an extremely high metabolic rate, with a maximum standardized uptake value greater than 10 owing to the considerable mitochondrial activity of the tumor. Liposarcomas show low to intermediate FDG uptake, with the value depending on histologic subtype. Pleomorphic liposarcomas demonstrate the most FDG uptake (median standardized uptake value, 4.6; range, 2.6–9.1), whereas well-differentiated liposarcomas display the least uptake (median standardized uptake value, 2.0; range, 1.2–3.2) (64). Thus, it has been proposed that high FDG uptake values in fat-containing lesions are suggestive of hibernomas. Hibernomas may also demonstrate fluctuation in standardized uptake values over time, another finding that may be helpful for differentiating hibernomas and malignant fatty tumors (69).

Retroperitoneal Myelolipomas

Extra-adrenal myelolipomas are benign lesions that are histologically identical to adrenal myelolipomas. They contain mature adipose cells and "trilineage" hematopoietic cells (red blood cells, white blood cells, and platelets) in distributions that are identical to those of normal bone marrow. They usually occur in the presacral region but have also been reported in the perinephric space (70). Presacral myelolipomas occur predominantly in elderly women (mean age, 65 years; ratio of women to men, 2:1) and are usually asymptomatic but may manifest with symptoms related to mass effect on the pelvic organs. The tumors may be large at presentation, ranging from 5 to 19 cm in diameter.

On US images, these tumors vary in their echogenic pattern and may be hyperechoic or hypoechoic, depending on the predominance of fat or hematopoietic elements, respectively. On CT images, they are well-circumscribed encapsulated fatty masses interspersed with avidly enhancing hematopoietic soft-tissue elements. The attenuation

value of fat in myelolipomas is usually higher than that of retroperitoneal fat because of the admixture with hematopoietic tissue (54). Areas of intratumoral hemorrhage or calcification may also be seen. On MR images, areas of high signal intensity on T1-weighted images and intermediate to high signal intensity on T2-weighted images with loss of signal intensity on fat-suppressed images confirm intratumoral fat (Fig 32). Myelolipomas show variable enhancement, depending on the proportion of hematopoietic tissue. Technetium 99m–sulfur colloid scintigraphy has been suggested to confirm the presence of erythroid elements in myelolipomas (71); however, it has not proven useful in the cases we have encountered.

The differential diagnosis for fat-containing presacral masses includes lipoma, liposarcoma, teratoma, extramedullary hematopoiesis, and lipomatosis. Unlike liposarcomas, myelolipomas are typically well defined and do not exhibit an infiltrative growth pattern. Teratomas are usually seen in younger individuals and contain fluid-filled cystic components, whereas myelolipomas are typically seen in elderly patients and do not show cystic changes. Differentiating presacral myelolipomas from other fat-containing lesions may not always be possible with imaging alone. Presacral myelolipomas occur predominantly in elderly women, which is the single most useful feature for differentiating this tumor from other fat-containing presacral lesions (72).

Retroperitoneal Fat-containing GCTs

Teratomas are GCTs that are commonly composed of multiple cell types, derived from one or more of the three germ cell layers. Teratomas that contain only one or two germ cell layer components are considered monodermal or bidermal, respectively. Primary retroperitoneal teratomas account for 1%–11% of retroperitoneal neoplasms and are most commonly found in neonates and young adults. About 1%–2.5% of GCTs originate in an extragonadal location from aberrant primordial germ cell rests; the retroperitoneum is the second most common extragonadal site for GCTs, after the mediastinum.

Mature Cystic Teratoma.—Primary retroperitoneal mature cystic teratomas are extremely rare. They are more common in female patients, with a female-to-male ratio of 3.4:1, and have a bimodal age distribution, with a peak in the first 6 months of life and a second peak in early adulthood (73). Typically, mature cystic teratoma appears as a well-circumscribed complex cystic mass that contains a variable amount of fluid, fat, or sebum in the form of a fat-fluid level and calcification in a congealed or linear strand pattern (Figs 33, 34) (73).

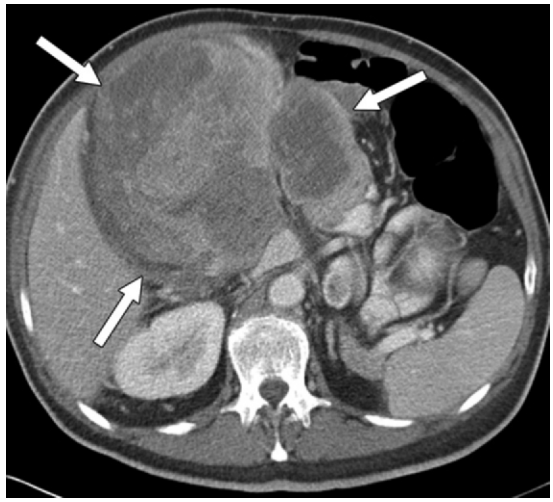

Figure 30. Pleomorphic liposarcoma in a 59-year-old man. Axial contrast-enhanced CT image shows a heterogeneous soft-tissue retroperitoneal mass (arrows) without detectable fat attenuation.

Figure 31. Lipoblastoma in a 3-year-old boy. Axial contrast-enhanced CT image shows a retroperitoneal mass (arrows) in the right abdomen. The mass has fat attenuation, fine soft-tissue septa, and an area of fluid attenuation (arrowhead) due to myxoid material.

While most mature cystic teratomas are benign, a variety of malignant components may be present or develop from clonal transformation. Primary retroperitoneal mature teratomas can rarely undergo malignant transformation. Adenocarcinoma is the most common somatic malignancy that arises in retroperitoneal mature cystic teratomas, as opposed to malignant transformation in ovarian mature cystic teratomas (in which squamous cell carcinoma occurs in most cases) (74).

Sacrococcygeal Teratoma.—Sacrococcygeal teratomas are commonly seen in infants and children, with a prevalence of approximately one in every 40 000 live births and a female-to-male ratio of about 4:1 (75). Sacrococcygeal teratoma rarely occurs in adults and its true incidence is

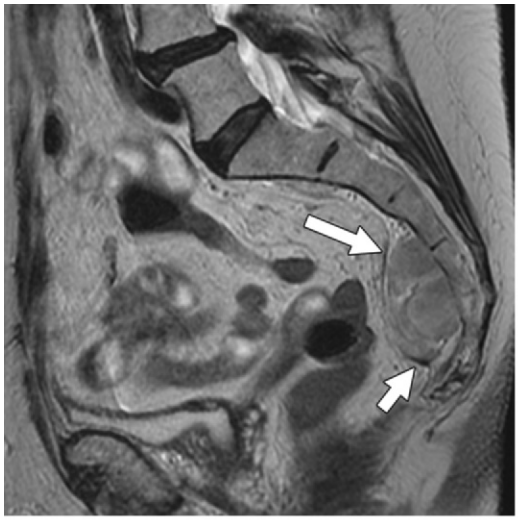

a.

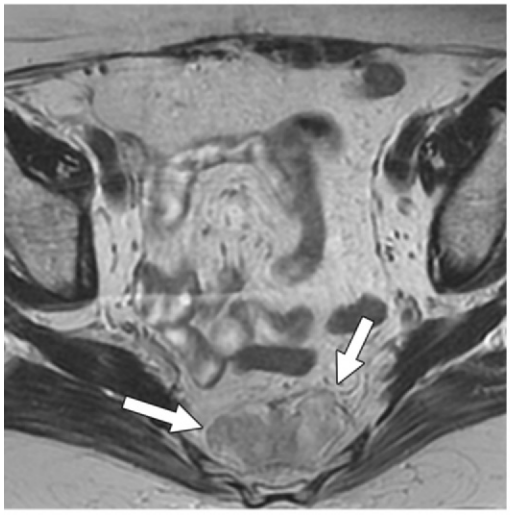

b.

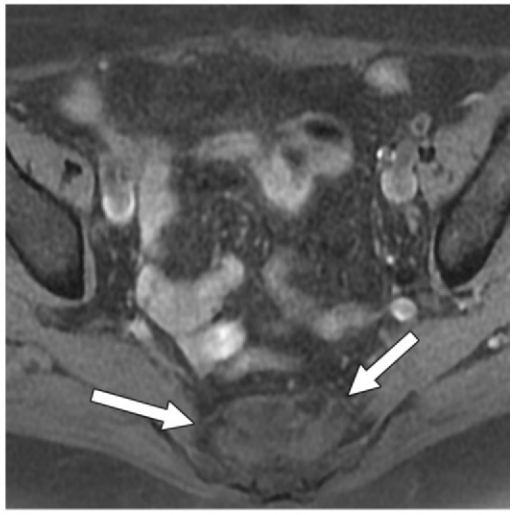

c.

Figure 32. Presacral myelolipoma in a 74-year-old woman. Sagittal T2-weighted MR image **(a)**, axial T1-weighted MR image **(b)**, and axial fat-suppressed T1-weighted MR image **(c)** show a lobulated presacral mass (arrows). The mass demonstrates heterogeneous predominantly high signal intensity relative to that of muscle in **a** and **b** and loss of signal intensity in **c**.

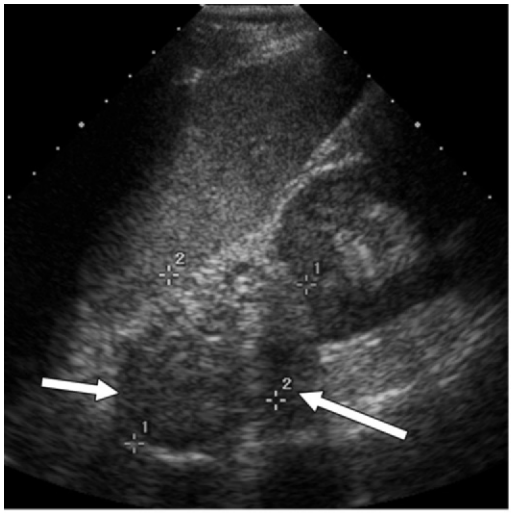

a.

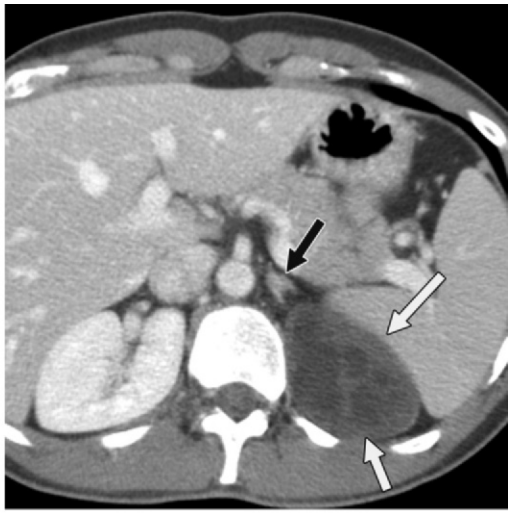

b.

Figure 33. Retroperitoneal mature cystic teratoma in a 34-year-old woman. **(a)** Sagittal US image shows a heterogeneous mass (arrows) superior to the left kidney. **(b)** Axial contrast-enhanced CT image shows the heterogeneous mass (white arrows) with cystic areas of fat attenuation. The mass is separate from the adrenal gland (black arrow).

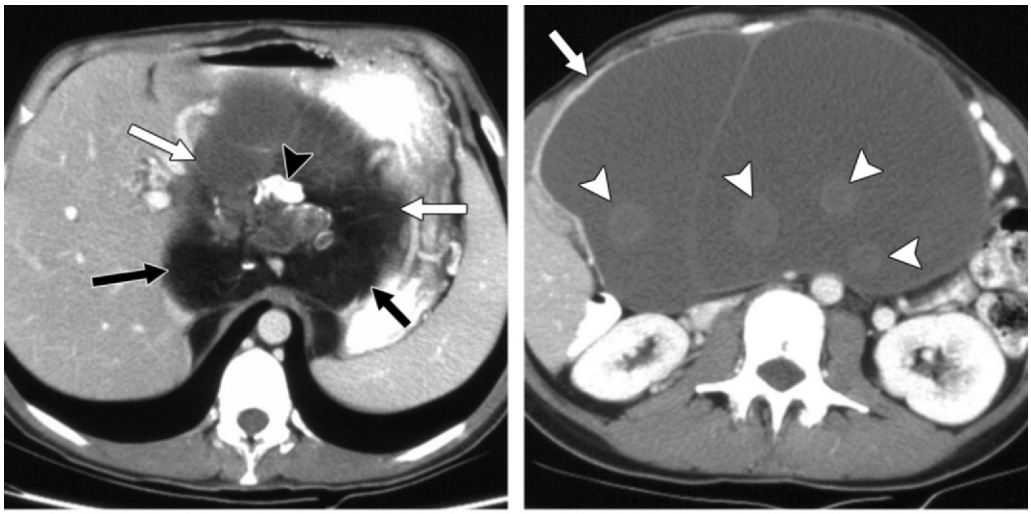

a. b.

Figure 34. Mature cystic teratoma in a 17-year-old girl. Axial contrast-enhanced discontiguous CT images of the upper abdomen show a complex mass (white arrows) that contains fat (black arrows in **a**), calcifications (arrowhead in **a**), and soft-tissue–attenuation rounded structures (arrowheads in **b**).

Figure 35. Retroperitoneal metastatic GCT in a 21-year-old man with a history of left testicular mixed GCT with components of immature teratoma. Axial contrast-enhanced CT image shows a predominantly solid left paraaortic mass (arrows) with scattered calcifications and foci of fat (arrowhead).

not known, but a review of the current literature demonstrates that fewer than 120 cases have been reported worldwide (76). In contrast to the neonatal presentation of sacrococcygeal teratomas, in which 90% are visible externally, most sacrococcygeal teratomas in adults manifest as intrapelvic masses. Clinically, presacral teratomas may be asymptomatic or may manifest as a pelvic mass, with recurrent pilonidal infections or pressure symptoms, including constipation. There is a 20%–30% risk for infection and a 1%–12% risk for malignant transformation in adult patients—usually adenocarcinoma (76,77). Because benign and malignant tissues can coexist within a sacrococcygeal teratoma, surgical excision and careful histopathologic analysis are necessary to exclude malignancy in adults. At imaging, sacrococcygeal teratomas may have varied appearances, ranging from cystic to solid masses; areas of intratumoral fat may also be seen.

Malignant Teratoma.—Most malignant retroperitoneal GCTs are metastases from primary gonadal GCTs, and they are seen in 30% of patients with primary gonadal GCTs (54). Careful US examination of the testes is crucial in every patient with a retroperitoneal GCT to evaluate the patient for primary testicular GCTs. Occasionally, the primary testicular tumor is not visible, or small intratesticular scars are found in patients with retroperitoneal GCTs; these scars represent regressed "burned out" GCTs (78). Gonadal GCTs that contain immature teratomatous elements can manifest as retroperitoneal masses that contain fat.

Retroperitoneal GCTs are usually large at presentation. The presenting symptoms and signs include a palpable mass with or without pain, weight loss, constipation, hip and back pain, dyspnea, leg edema, fever, varicocele, and urinary retention. Encasement, displacement, and compression of the abdominal vessels are common. On images, both primary and metastatic malignant teratomas appear as enhancing soft-tissue masses with foci of fat and calcifications (Fig 35).

Retroperitoneal Paraganglioma

Retroperitoneal paragangliomas arise predominantly from the paraganglia, which are symmetrically distributed along the abdominal aorta and are closely related to the sympathetic nervous system (79). The retroperitoneum accounts for 85% of all extra-adrenal paragangliomas. In the retroperitoneum, the most common site for paragangliomas is the organ of Zuckerkandl, which is located anterior to the aorta at the level of the origin of the inferior mesenteric artery (80).

Paragangliomas are commonly seen in the 3rd–4th decades of life, with no sex predilection. They can be associated with type 1 neurofibromatosis, multiple endocrine neoplasia syndrome, and von Hippel–Lindau disease. There is an increased incidence of extra-adrenal paragangliomas in patients with genetic mutations within the succinate dehydrogenase B subunit and the succinate dehydrogenase D subunit. Extra-adrenal paragangliomas are more likely to be malignant (40%) than are adrenal pheochromocytomas (2%–11%). Patients with functioning paragangliomas (40%) present with a variety of symptoms that result from catecholamine excess, including headaches, palpitation, excessive sweating, tremor, vomiting, chest pain, constipation, and visual disturbances. Patients with nonfunctioning paragangliomas usually present late after disease onset, with symptoms resulting from compression of surrounding structures. Rarely, paraganglioma can manifest with acute abdomen caused by retroperitoneal hemorrhage.

On CT images, paraganglioma is usually seen as a large, well-defined, avidly enhancing tumor with areas of hemorrhage and necrosis. The tumor is highly vascular, and large vessels can be seen around it. Punctate calcification is seen in 15% of cases, and a fluid-fluid level can be seen due to intratumoral hemorrhage. On MR images, paragangliomas are usually hypointense or isointense compared with the liver parenchyma, with signal voids on T1-weighted images. Small tumors are markedly hyperintense, while larger tumors usually show variable signal intensity on T2-weighted MR images. Radionuclide imaging performed after administration of *m*-iodobenzylguanidine shows high uptake in paragangliomas and is a sensitive technique for localizing these lesions in patients who present with suggestive symptoms and who show laboratory evidence of catecholamine excess (79,81). As with adrenal pheochromocytoma, microscopic and macroscopic fat is rarely found in retroperitoneal paraganglioma (16).

Extramedullary Hematopoiesis

Extramedullary hematopoiesis is characterized by abnormal deposits of hematopoietic tissue outside the bone marrow as a compensatory mechanism for inefficient hematopoiesis by the bone marrow. Although extramedullary hematopoiesis is not a true neoplasm, it can manifest as a mass in the retroperitoneum. The condition is seen in hemoglobinopathy, myelofibrosis, leukemia, lymphoma, and carcinoma. The retroperitoneum is an uncommon site for extramedullary hematopoiesis, which is typically found in the liver, spleen, and lymph nodes. Common sites of involvement in the retroperitoneum include the paravertebral, perinephric, and presacral regions. Perinephric involvement of extramedullary hematopoiesis is rare and appears as soft-tissue masses intermixed with fat or as a diffuse uniform infiltrative process that surrounds the kidneys (82,83). Splenectomy may have a role in accelerating development of extramedullary hematopoiesis in uncommon sites (82). The presence of fat in extramedullary hematopoiesis masses is indicative of old inactive lesions. The typical CT appearance is round or lobulated masses with soft-tissue attenuation, with or without macroscopic fat. The MR imaging appearance varies and depends on the relative proportion of active and inactive marrow. Active extramedullary red marrow usually appears as a well-demarcated isointense or hypointense mass on T1- and T2-weighted images. After contrast material administration, there is always some enhancement in active extramedullary hematopoiesis lesions. Areas of fatty infiltration within old inactive disease demonstrate high signal intensity on T1- and T2-weighted images. Areas of low signal intensity can be seen on T1- and T2-weighted images because of the red marrow or hemosiderin content (84). The diagnosis is evident when the patient has a known history of hemoglobinopathy, hepatosplenomegaly, and characteristic skeletal changes of a marrow infiltrative process (54).

Retroperitoneal Ganglioneuroma

Ganglioneuromas are rare tumors that arise from the autonomic ganglion cells of the peripheral nervous system—usually the sympathetic ganglion. They represent the benign end of the spectrum for the ganglion cell lineage, whereas ganglioneuroblastomas and neuroblastomas comprise the malignant counterparts. Ganglioneuromas may arise anywhere along the peripheral autonomic ganglion sites but are most common within the posterior mediastinum (39%–43% of cases) and retroperitoneum (32%–52% of cases). Less commonly, they may arise in the adrenal medulla, parapharyngeal region, visceral ganglia, or cranial nerve ganglia. They are usually asymptomatic but can manifest with pain or a mass. Ganglioneuromas occasionally secrete hormones such as catecholamines,

vasoactive intestinal peptides, or androgenic hormones. This tumor is commonly seen in the 20–40-year-old age group, with no sex predilection. Histopathologically, ganglioneuromas are composed of Schwann cells, ganglion cells, and nerve fibers. In the retroperitoneum, the tumor is commonly seen along the paravertebral sympathetic ganglia (59% of cases) or, less commonly, in the adrenal medulla. Lipomatous ganglioneuroma, previously called "ganglioneuroma with fatty replacement," is an extremely rare variant of ganglioneuroma that was first reported in 1999 by Hara et al (85). It is characterized by a mature adipocytic component admixed with conventional ganglioneuromas (86–89). The presence of fat can be explained by adipocytic differentiation or lipometaplasia (86).

On CT images, ganglioneuroma is depicted as a well-circumscribed, lobulated, hypoattenuating mass that may surround a blood vessel without narrowing the lumen (Fig 36). Ganglioneuromas may grow through the adjacent intervertebral neuroforamen and extend into the spinal canal with a "dumbbell" or "hourglass" configuration. Discrete punctate calcifications are seen in 20%–30% of ganglioneuromas. Necrosis and hemorrhage are uncommon. The presence of fat is unusual; when present, it appears as locules of fat attenuation intermingled with soft-tissue components or peripheral fat replacement surrounding soft-tissue elements (90). After contrast material administration, ganglioneuromas usually demonstrate characteristic mild enhancement during the arterial phase and progressive delayed retention of contrast material on delayed phase images. On MR images, a ganglioneuroma is homogeneously hypointense on T1-weighted images, with varying signal intensity on T2-weighted images depending on the myxoid, cellular, and collagen components. A whorled appearance on MR images has been reported and is due to interlacing bundles of longitudinal and transverse Schwann cells or collagen fibers. Generally, ganglioneuromas are larger and have more calcification than do nerve sheath tumors. The prognosis is good after surgical resection.

Figure 36. Retroperitoneal ganglioneuroma in a 55-year-old man. Axial contrast-enhanced late arterial phase CT image shows a well-circumscribed retroperitoneal soft-tissue mass (black arrows) encasing the superior mesenteric artery. The mass contains a focal area of macroscopic fat (white arrow).

Conclusion

The relationship between a retroperitoneal mass and the retroperitoneal organs determines whether the mass arises from or displaces neighboring organs. Fat is easily recognized because of its characteristic imaging appearance, and its presence within a retroperitoneal lesion helps in refining the differential diagnosis. Most fat-containing retroperitoneal lesions can be characterized on the basis of a patient's demographics, clinical presentation, and imaging features. When there is any doubt, imaging can guide percutaneous biopsy to obtain tissue for pathologic examination.

Acknowledgments.—Special thanks to Kent Sanders, MD, for the medical illustrations.

Disclosures of Conflicts of Interest.—**M.T.** *Activities related to the present article:* disclosed no relevant relationships. *Activities not related to the present article:* royalties and consulting fees from Amirsys. *Other activities:* disclosed no relevant relationships.

References

1. Hamer OW, Aguirre DA, Casola G, Lavine JE, Woenckhaus M, Sirlin CB. Fatty liver: imaging patterns and pitfalls. RadioGraphics 2006;26(6):1637–1653.
2. Nishino M, Hayakawa K, Minami M, Yamamoto A, Ueda H, Takasu K. Primary retroperitoneal neoplasms: CT and MR imaging findings with anatomic and pathologic diagnostic clues. RadioGraphics 2003;23(1):45–57.
3. Kloos RT, Gross MD, Francis IR, Korobkin M, Shapiro B. Incidentally discovered adrenal masses. Endocr Rev 1995;16(4):460–484.
4. Park SH, Kim MJ, Kim JH, Lim JS, Kim KW. Differentiation of adrenal adenoma and nonadenoma in unenhanced CT: new optimal threshold value and the usefulness of size criteria for differentiation. Korean J Radiol 2007;8(4):328–335.
5. Caoili EM, Korobkin M, Francis IR, et al. Adrenal masses: characterization with combined unenhanced and delayed enhanced CT. Radiology 2002;222(3):629–633.
6. Fujiyoshi F, Nakajo M, Fukukura Y, Tsuchimochi S. Characterization of adrenal tumors by chemical shift fast low-angle shot MR imaging: comparison of four methods of quantitative evaluation. AJR Am J Roentgenol 2003;180(6):1649–1657.
7. Papotti M, Sapino A, Mazza E, Sandrucci S, Volante M, Bussolati G. Lipomatous changes in adrenocortical adenomas: report of two cases. Endocr Pathol 1996;7(3):223–228.
8. Kenney PJ, Wagner BJ, Rao P, Heffess CS. Myelolipoma: CT and pathologic features. Radiology 1998;208(1):87–95.
9. Ioannidis O, Papaemmanouil S, Chatzopoulos S, et al. Giant bilateral symptomatic adrenal myelolipomas associated with congenital adrenal hyperplasia. Pathol Oncol Res 2011;17(3):775–778.

10. Nermoen I, Rørvik J, Holmedal SH, et al. High frequency of adrenal myelolipomas and testicular adrenal rest tumours in adult Norwegian patients with classical congenital adrenal hyperplasia because of 21-hydroxylase deficiency. Clin Endocrinol (Oxf) 2011;75(6):753–759.
11. Almeida MQ, Kaupert LC, Brito LP, et al. Increased expression of ACTH (MC2R) and androgen (AR) receptors in giant bilateral myelolipomas from patients with congenital adrenal hyperplasia. BMC Endocr Disord 2014;14:42.
12. Mittendorf EA, Evans DB, Lee JE, Perrier ND. Pheochromocytoma: advances in genetics, diagnosis, localization, and treatment. Hematol Oncol Clin North Am 2007;21(3):509–525, ix.
13. Taffel M, Haji-Momenian S, Nikolaidis P, Miller FH. Adrenal imaging: a comprehensive review. Radiol Clin North Am 2012;50(2):219–243, v.
14. Elsayes KM, Narra VR, Leyendecker JR, Francis IR, Lewis JS Jr, Brown JJ. MRI of adrenal and extraadrenal pheochromocytoma. AJR Am J Roentgenol 2005;184(3):860–867.
15. Patel J, Davenport MS, Cohan RH, Caoili EM. Can established CT attenuation and washout criteria for adrenal adenoma accurately exclude pheochromocytoma? AJR Am J Roentgenol 2013;201(1):122–127.
16. Blake MA, Kalra MK, Maher MM, et al. Pheochromocytoma: an imaging chameleon. RadioGraphics 2004;24(suppl 1):S87–S99.
17. Ganeshan D, Bhosale P, Kundra V. Current update on cytogenetics, taxonomy, diagnosis, and management of adrenocortical carcinoma: what radiologists should know. AJR Am J Roentgenol 2012;199(6):1283–1293.
18. Bharwani N, Rockall AG, Sahdev A, et al. Adrenocortical carcinoma: the range of appearances on CT and MRI. AJR Am J Roentgenol 2011;196(6):W706–W714.
19. Ferrozzi F, Bova D. CT and MR demonstration of fat within an adrenal cortical carcinoma. Abdom Imaging 1995;20(3):272–274.
20. Shumaker NR, Rochman CM, Legallo RD, Northup CJ, Hanks JB. Incidentally identified adrenal lipoma: case report and review of related literature. Endocr Pract 2008;14(2):209–212.
21. Yarmish G, DiPoce J. Case 199: aggressive angiomyolipoma with renal vein thrombosis and pulmonary fat embolus. Radiology 2013;269(2):615–618.
22. Schieda N, Avruch L, Flood TA. Small (<1 cm) incidental echogenic renal cortical nodules: chemical shift MRI outperforms CT for confirmatory diagnosis of angiomyolipoma (AML). Insights Imaging 2014;5(3):295–299.
23. Israel GM, Hindman N, Hecht E, Krinsky G. The use of opposed-phase chemical shift MRI in the diagnosis of renal angiomyolipomas. AJR Am J Roentgenol 2005;184(6):1868–1872.
24. Kim JK, Park SY, Shon JH, Cho KS. Angiomyolipoma with minimal fat: differentiation from renal cell carcinoma at biphasic helical CT. Radiology 2004;230(3):677–684.
25. Ferré R, Cornelis F, Verkarre V, et al. Double-echo gradient chemical shift MR imaging fails to differentiate minimal fat renal angiomyolipomas from other homogeneous solid renal tumors. Eur J Radiol 2015;84(3):360–365.
26. Hindman N, Ngo L, Genega EM, et al. Angiomyolipoma with minimal fat: can it be differentiated from clear cell renal cell carcinoma by using standard MR techniques? Radiology 2012;265(2):468–477.
27. Schieda N, Kielar AZ, Al Dandan O, McInnes MD, Flood TA. Ten uncommon and unusual variants of renal angiomyolipoma (AML): radiologic-pathologic correlation. Clin Radiol 2015;70(2):206–220.
28. Yang CW, Shen SH, Chang YH, et al. Are there useful CT features to differentiate renal cell carcinoma from lipid-poor renal angiomyolipoma? AJR Am J Roentgenol 2013;201(5):1017–1028.
29. Chen CL, Tang SH, Wu ST, et al. Calcified, minimally fat-contained angiomyolipoma clinically indistinguishable from a renal cell carcinoma. BMC Nephrol 2013;14:160.
30. Ellingson JJ, Coakley FV, Joe BN, Qayyum A, Westphalen AC, Yeh BM. Computed tomographic distinction of perirenal liposarcoma from exophytic angiomyolipoma: a feature analysis study. J Comput Assist Tomogr 2008;32(4):548–552.
31. Hélénon O, Merran S, Paraf F, et al. Unusual fat-containing tumors of the kidney: a diagnostic dilemma. RadioGraphics 1997;17(1):129–144.
32. Aron M, Aydin H, Sercia L, Magi-Galluzzi C, Zhou M. Renal cell carcinomas with intratumoral fat and concomitant angiomyolipoma: potential pitfalls in staging and diagnosis. Am J Clin Pathol 2010;134(5):807–812.
33. Garin JM, Marco I, Salva A, Serrano F, Bondia JM, Pacheco M. CT and MRI in fat-containing papillary renal cell carcinoma. Br J Radiol 2007;80(957):e193–e195.
34. Wasser EJ, Shyn PB, Riveros-Angel M, Sadow CA, Steele GS, Silverman SG. Renal cell carcinoma containing abundant non-calcified fat. Abdom Imaging 2013;38(3):598–602.
35. Hélénon O, Chrétien Y, Paraf F, Melki P, Denys A, Moreau JF. Renal cell carcinoma containing fat: demonstration with CT. Radiology 1993;188(2):429–430.
36. Richmond L, Atri M, Sherman C, Sharir S. Renal cell carcinoma containing macroscopic fat on CT mimics an angiomyolipoma due to bone metaplasia without macroscopic calcification. Br J Radiol 2010;83(992):e179–e181.
37. Silverman SG, Gan YU, Mortele KJ, Tuncali K, Cibas ES. Renal masses in the adult patient: the role of percutaneous biopsy. Radiology 2006;240(1):6–22.
38. Silverman SG, Israel GM, Herts BR, Richie JP. Management of the incidental renal mass. Radiology 2008;249(1):16–31.
39. Ke HL, Hsiao HL, Guh JY, Liu CS, Huang CH, Wu WJ. Primary intrarenal lipoma: a case report. Kaohsiung J Med Sci 2005;21(8):383–386.
40. Liu X, Wu X, He D, et al. The first case of renal lipoma in a child. J Pediatr Surg 2011;46(6):1281–1283.
41. Chiang IC, Jang MY, Tsai KB, Hsieh TJ. Huge renal lipoma with prominent hypervascular non-adipose elements. Br J Radiol 2006;79(946):e148–e151.
42. Shastri C, Kumar J, Jaiswal S, Mandhani A. Renal dedifferentiated liposarcoma with intra-caval tumor thrombus: a rare case. Indian J Urol 2012;28(2):208–210.
43. Subramanyam BR, Bosniak MA, Horii SC, Megibow AJ, Balthazar EJ. Replacement lipomatosis of the kidney: diagnosis by computed tomography and sonography. Radiology 1983;148(3):791–792.
44. Andersen PE, Thorlund MG, Wennevik GE, Pedersen RL, Lund L. Interventional treatment of renal angiomyolipoma: immediate results and clinical and radiological follow-up of 4.5 years. Acta Radiol Open 2015;4(7):2058460115592442.
45. Gossner J. Pancreatic lipomas: prevalence in patients undergoing abdominal CT. Pol J Radiol 2014;79:259–261.
46. Lane J, Vance A, Finelli D, Williams G, Ravichandran P. Dermoid cyst of the pancreas: a case report with literature review. J Radiol Case Rep 2012;6(12):17–25.
47. Jacobs JE, Dinsmore BJ. Mature cystic teratoma of the pancreas: sonographic and CT findings. AJR Am J Roentgenol 1993;160(3):523–524.
48. Degrate L, Misani M, Mauri G, et al. Mature cystic teratoma of the pancreas: case report and review of the literature of a rare pancreatic cystic lesion. JOP 2012;13(1):66–72.
49. Kim HJ, Byun JH, Park SH, et al. Focal fatty replacement of the pancreas: usefulness of chemical shift MRI. AJR Am J Roentgenol 2007;188(2):429–432.
50. King LJ, Scurr ED, Murugan N, Williams SG, Westaby D, Healy JC. Hepatobiliary and pancreatic manifestations of cystic fibrosis: MR imaging appearances. RadioGraphics 2000;20(3):767–777.
51. Robertson MB, Choe KA, Joseph PM. Review of the abdominal manifestations of cystic fibrosis in the adult patient. RadioGraphics 2006;26(3):679–690.
52. Matsumoto S, Mori H, Miyake H, et al. Uneven fatty replacement of the pancreas: evaluation with CT. Radiology 1995;194(2):453–458.
53. Heyns CF. Pelvic lipomatosis: a review of its diagnosis and management. J Urol 1991;146(2):267–273.
54. Rajiah P, Sinha R, Cuevas C, Dubinsky TJ, Bush WH Jr, Kolokythas O. Imaging of uncommon retroperitoneal masses. RadioGraphics 2011;31(4):949–976.
55. Alves MD, Brites C, Sprinz E. HIV-associated lipodystrophy: a review from a Brazilian perspective. Ther Clin Risk Manag 2014;10:559–566.

56. Colomer Rubio E, Blanes Gallego A, Carbonell Biot C, Villar Grimalt A, Tomás Ivorra H, Llamusí Lorente A. Mesenteric panniculitis with retroperitoneal involvement resolved after treatment with intravenous cyclophosphamide pulses [in Spanish]. Med Interna 2003;20(1):31–33.
57. Sabaté JM, Torrubia S, Maideu J, Franquet T, Monill JM, Pérez C. Sclerosing mesenteritis: imaging findings in 17 patients. AJR Am J Roentgenol 1999;172(3):625–629.
58. Bakker OJ, van Santvoort H, Besselink MG, et al. Extrapancreatic necrosis without pancreatic parenchymal necrosis: a separate entity in necrotising pancreatitis? Gut 2013;62(10):1475–1480.
59. Chen H, Tsang Y, Wu C, Su C, Hsu JC. Perirenal fat necrosis secondary to hemorrhagic pancreatitis, mimicking retroperitoneal liposarcoma: CT manifestation. Abdom Imaging 1996;21(6):546–548.
60. Gupta P, Bhattatiry M, Eshaghi N, Tirkes A, Kumar M. Idiopathic retroperitoneal fat necrosis in a patient on long-term steroids. The Internet Journal of Radiology 2004;4(1). http://ispub.com/IJRA/4/1/6989. Accessed February 10, 2016.
61. Upadhyaya VS, Uppoor R, Shetty L. Mammographic and sonographic features of fat necrosis of the breast. Indian J Radiol Imaging 2013;23(4):366–372.
62. Lee SA, Chung HW, Cho KJ, et al. Encapsulated fat necrosis mimicking subcutaneous liposarcoma: radiologic findings on MR, PET-CT, and US imaging. Skeletal Radiol 2013;42(10):1465–1470.
63. Kamaya A, Federle MP, Desser TS. Imaging manifestations of abdominal fat necrosis and its mimics. RadioGraphics 2011;31(7):2021–2034.
64. Craig WD, Fanburg-Smith JC, Henry LR, Guerrero R, Barton JH. Fat-containing lesions of the retroperitoneum: radiologic-pathologic correlation. RadioGraphics 2009;29(1):261–290.
65. Song T, Shen J, Liang BL, Mai WW, Li Y, Guo HC. Retroperitoneal liposarcoma: MR characteristics and pathological correlative analysis. Abdom Imaging 2007;32(5):668–674.
66. Murphey MD, Arcara LK, Fanburg-Smith J. Imaging of musculoskeletal liposarcoma with radiologic-pathologic correlation. RadioGraphics 2005;25(5):1371–1395.
67. Xu Y, Wang J, Peng Y, Zeng J. CT characteristics of primary retroperitoneal neoplasms in children. Eur J Radiol 2010;75(3):321–328.
68. Colville J, Feigin K, Antonescu CR, Panicek DM. Hibernoma: report emphasizing large intratumoral vessels and high T1 signal. Skeletal Radiol 2006;35(7):547–550.
69. Smith CS, Teruya-Feldstein J, Caravelli JF, Yeung HW. False-positive findings on 18F-FDG PET/CT: differentiation of hibernoma and malignant fatty tumor on the basis of fluctuating standardized uptake values. AJR Am J Roentgenol 2008;190(4):1091–1096.
70. Temizoz O, Genchellac H, Demir MK, Unlu E, Ozdemir H. Bilateral extra-adrenal perirenal myelolipomas: CT features. Br J Radiol 2010;83(994):e198–e199.
71. Nguyen BD. Retroperitoneal extraadrenal myelolipoma: technetium-99m sulfur colloid scintigraphy and CT imaging. Clin Nucl Med 2007;32(2):135–138.
72. Shanbhogue AK, Fasih N, Macdonald DB, Sheikh AM, Menias CO, Prasad SR. Uncommon primary pelvic retroperitoneal masses in adults: a pattern-based imaging approach. RadioGraphics 2012;32(3):795–817.
73. Davidson AJ, Hartman DS, Goldman SM. Mature teratoma of the retroperitoneum: radiologic, pathologic, and clinical correlation. Radiology 1989;172(2):421–425.
74. Hong W, Dumoff KL, Torigian DA, Bing Z. Primary retroperitoneal mature cystic teratoma with focal enteric type adenocarcinoma in a post-partum woman: report of a case with literature review. Rare Tumors 2013;5(1):e1.
75. Valdiserri RO, Yunis EJ. Sacrococcygeal teratomas: a review of 68 cases. Cancer 1981;48(1):217–221.
76. Simpson PJ, Wise KB, Merchea A, et al. Surgical outcomes in adults with benign and malignant sacrococcygeal teratoma: a single-institution experience of 26 cases. Dis Colon Rectum 2014;57(7):851–857.
77. Chêne G, Voitellier M. Benign pre-sacral teratoma and vestigial retrorectal cysts in the adult [in French]. J Chir (Paris) 2006;143(5):310–314.
78. Tasu JP, Faye N, Eschwege P, Rocher L, Bléry M. Imaging of burned-out testis tumor: five new cases and review of the literature. J Ultrasound Med 2003;22(5):515–521.
79. Lee KY, Oh YW, Noh HJ, et al. Extraadrenal paragangliomas of the body: imaging features. AJR Am J Roentgenol 2006;187(2):492–504.
80. Disick GI, Palese MA. Extra-adrenal pheochromocytoma: diagnosis and management. Curr Urol Rep 2007;8(1):83–88.
81. Sahdev A, Sohaib A, Monson JP, Grossman AB, Chew SL, Reznek RH. CT and MR imaging of unusual locations of extra-adrenal paragangliomas (pheochromocytomas). Eur Radiol 2005;15(1):85–92.
82. Khandelwal A, Gupta A, Khandelwal K. Perinephric extramedullary hematopoiesis. Kidney Int 2012;81(3):326.
83. Georgiades CS, Neyman EG, Francis IR, Sneider MB, Fishman EK. Typical and atypical presentations of extramedullary hemopoiesis. AJR Am J Roentgenol 2002;179(5):1239–1243.
84. Tsitouridis J, Stamos S, Hassapopoulou E, Tsitouridis K, Nikolopoulos P. Extramedullary paraspinal hematopoiesis in thalassemia: CT and MRI evaluation. Eur J Radiol 1999;30(1):33–38.
85. Hara M, Ohba S, Andoh K, et al. A case of ganglioneuroma with fatty replacement: CT and MRI findings. Radiat Med 1999;17(6):431–434.
86. Adachi S, Kawamura N, Hatano K, et al. Lipomatous ganglioneuroma of the retroperitoneum. Pathol Int 2008;58(3):183–186.
87. Duffy S, Jhaveri M, Scudierre J, Cochran E, Huckman M. MR imaging of a posterior mediastinal ganglioneuroma: fat as a useful diagnostic sign. AJNR Am J Neuroradiol 2005;26(10):2658–2662.
88. Guan YB, Zhang WD, Zeng QS, Chen GQ, He JX. CT and MRI findings of thoracic ganglioneuroma. Br J Radiol 2012;85(1016):e365–e372.
89. Meng QD, Ma XN, Wei H, Pan RH, Jiang W, Chen FS. Lipomatous ganglioneuroma of the retroperitoneum. Asian J Surg 2013S1015-9584(13)00068-7.
90. Yorita K, Yonei A, Ayabe T, et al. Posterior mediastinal ganglioneuroma with peripheral replacement by white and brown adipocytes resulting in diagnostic fallacy from a false-positive 18F-2-fluoro-2-deoxyglucose-positron emission tomography finding: a case report. J Med Case Reports 2014;8:345.